Dayside ELF electromagnetic wave survey: A Polar statistical study of chorus and hiss

Bruce T. Tsurutani,[1] Barbara J. Falkowski,[1,2] Olga P. Verkhoglyadova,[1,3] Jolene S. Pickett,[4] Ondrej Santolík,[5,6] and Gurbax S. Lakhina[7]

Received 20 September 2011; revised 25 June 2012; accepted 25 June 2012; published 23 August 2012.

[1] Statistical analyses of Polar plasma wave data are performed to determine the occurrence frequency, intensity, and Poynting direction of ~360 Hz to ~1.8 kHz extremely low-frequency (ELF) electromagnetic waves (chorus, magnetosonic mode, and hiss) in the dayside sector of the magnetosphere. The study is limited to an L* range of 2 to 9 and a magnetic local time (MLT) range of 0900 to 1500, a region infrequently covered in past statistical surveys. The study was performed on 1996–1997 data, an interval near solar minimum. It is determined that in the outer region of the magnetosphere, from L* = 6 to 9, the ~360 to ~800 Hz waves at Polar altitudes are typically characterized by downward (toward Earth) propagation. The downgoing waves have been previously identified as chorus in Tsurutani et al. (2011). The downgoing chorus have intensities of $\sim 10^{-2}$ nT^2, are right-hand circularly polarized and are propagating close to parallel to the ambient magnetic field B_0. The high rate of occurrence of these downward propagating waves narrows to a smaller region of L* = 6 to 7 for ~1.2 kHz waves.

In the inner region of the magnetosphere, L* = 3 to 6, the ~360 to 800 Hz waves are characteristically oblique (to B_0) and upwards propagating, away from the Earth. The upcoming waves are most likely plasmaspheric hiss and low altitude magnetospherically reflected waves. These waves are an order of magnitude less intense and less coherent than the downward propagating chorus waves. At low frequencies, ~360 Hz, there is a region near L* = 4 to 5, where obliquely propagating waves are detected. These are most probably a mixture of obliquely propagating plasmaspheric hiss and magnetosonic waves.

A detailed (case study) examination of upward propagating waves is made for one Polar pass to add context to the statistical results. The upward propagating waves are quasicoherent and slightly elliptically polarized at Polar altitudes. From this and the statistical results, we ascribe to the scenario that ~360 to 800 Hz chorus enters the plasmasphere at low altitude entry points and propagates through the plasmasphere as semicoherent hiss, in basic agreement with the Bortnik et al. (2008, 2009a) hypothesis for the origin of some plasmaspheric hiss. However, for ~1.2 and 1.8 kHz waves inside the nominal location of the plasmasphere, downward propagating waves have higher intensities than upward propagating or oblique waves, perhaps indicating effects associated with different source locations, different entry points and different reflection regions and/or damping/amplification. At ~800 Hz and ~1.2 kHz upward propagating waves with weak intensities are common in the range L* = 8–9. These may be chorus waves magnetospherically reflected to larger L*. For frequencies above ~1.5 kHz, most wave events are low intensity and upward propagating. It is possible that sferics and power line harmonics are contributors to these signals.

Citation: Tsurutani, B. T., B. J. Falkowski, O. P. Verkhoglyadova, J. S. Pickett, O. Santolík, and G. S. Lakhina (2012), Dayside ELF electromagnetic wave survey: A Polar statistical study of chorus and hiss, *J. Geophys. Res.*, *117*, A00L12, doi:10.1029/2011JA017180.

[1]Jet Propulsion Laboratory, California Institute of Technology, Pasadena, California, USA.

Corresponding author: B. T. Tsurutani, Jet Propulsion Laboratory, California Institute of Technology, Pasadena, CA 91109, USA. (bruce.t.tsurutani@jpl.nasa.gov)

0148-0227/12/2011JA017180

[2]Physics and Astronomy Departments, Glendale City College, Glendale, California, USA.
[3]CSPAR, University of Alabama, Huntsville, Alabama, USA.
[4]Department of Physics and Astronomy, University of Iowa, Iowa City, Iowa, USA.
[5]Institute of Atmospheric Physics, Prague, Czech Republic.
[6]Faculty of Mathematics and Physics, Charles University, Prague, Czech Republic.
[7]Indian Institute of Geomagnetism, Navi Mumbai, India.

1. Introduction

[2] A variety of ELF electromagnetic waves are present in the Earth's dayside magnetosphere. There is chorus in the outer zone [*Tsurutani and Smith*, 1974, 1977; *Anderson and Maeda*, 1977; *Koons and Roeder*, 1990; *Meredith et al.*, 2001, 2003; *Bortnik et al.*, 2009a, 2009b; *Li et al.*, 2009; *Tsurutani et al.*, 2009; *Sigsbee et al.*, 2010; *Haque et al.*, 2010; *Santolík et al.*, 2010a; *Wang et al.*, 2011], hiss inside the plasmasphere [*Thorne et al.*, 1973, 1977; *Smith et al.*, 1974; *Parrot and Lefeuvre*, 1986; *Storey et al.*, 1991; *Hayakawa and Sazhin*, 1992; *Meredith et al.*, 2006; *Bortnik et al.*, 2008, 2009a, 2009b], and magnetosonic waves at and near the plasmapause [*Gurnett*, 1976; *Perraut et al.*, 1982; *Olsen et al.*, 1987; *Boardsen et al.*, 1992; *Kasahara et al.*, 1994; *André et al.*, 2002; *Santolík et al.*, 2002, 2004a; *Němec et al.*, 2005, 2006a; *Meredith et al.*, 2008; *Pokhotelov et al.*, 2008]. All of these three waves propagate in or are related to the whistler mode. Chorus and magnetosonic waves have been considered to be important for wave-particle interaction mechanisms which lead to the acceleration of relativistic electrons [*Horne*, 2007; *Horne et al.*, 2007; *Summers et al.*, 2007a, 2007b; *Furuya et al.*, 2008; *Meredith et al.*, 2011].

[3] The chorus generation mechanism has been shown to be the electron loss cone/temperature anisotropy whistler mode instability [*Kennel and Petschek*, 1966; *Tsurutani et al.*, 1979; *Tsurutani and Lakhina*, 1997; *Schriver et al.*, 2010], while the mechanism for generation of proton cyclotron harmonic "magnetosonic" waves are thought to be a proton cyclotron instability driven by anisotropic ~5–30 keV protons with ring distributions [*Olsen et al.*, 1987; *Perraut et al.*, 1982; *Laakso et al.*, 1990; *Boardsen et al.*, 1992; *Horne et al.*, 2000; *Meredith et al.*, 2008]. The plasmaspheric hiss generation mechanism or mechanisms are less clear. *Thorne et al.* [1979] have suggested that hiss is generated in the plasmasphere by cyclical multipath circulation and near-equatorial local amplification. *Church and Thorne* [1983] were the first to argue that recirculation alone was insufficient to account for plasmaspheric hiss. An embryonic wave is thought to be needed as a "starter." *Chum and Santolík* [2005] have suggested that chorus may propagate into the plasmasphere and contribute to plasmaspheric hiss. *Bortnik et al.* [2008, 2009a, 2009b] suggested that plasmaspheric hiss is outer zone chorus that has propagated into the plasmasphere.

[4] Wave-particle interactions can lead to both relativistic electron acceleration [*Summers et al.*, 1998, 2004; *Albert*, 2000, 2002; *Horne*, 2002; *Horne et al.*, 2005; *Tsurutani et al.*, 2006a, and references therein; *Kasahara et al.*, 2009] as well as ~5 to 100 keV electron losses [*Tsurutani et al.*, 1975, 2009, 2011; *Horne et al.*, 2003; *Rodger et al.*, 2007; *Meredith et al.*, 2007; *Clilverd et al.*, 2007; *Lam et al.*, 2007; *Shprits*, 2009; *Lakhina et al.*, 2010]. For accurate modeling work, wave intensities, absolute directions of propagation, wave coherency and the wave direction of propagation relative to the ambient magnetic field, B_0, are needed. The purpose of this paper is to provide this information for the dayside sector (0900 to 1500 MLT) magnetosphere from L* = 2 to 9. We will use ~1 1/2 years of Polar plasma wave data from 1 April 1996 to 15 September 1997 [*Gurnett et al.*, 1995] to perform this study. Since Polar's orbit makes a complete rotation in MLT twice each 6 months, this ~1 1/2 year interval corresponds to ~6 passes through the local time region. It is shown that using the Poynting flux [*Santolík et al.*, 2010a] intensity and directional information orders the survey data nicely. This paper uses the same wave data set as in *Tsurutani et al.* [2011] and is complementary to the results presented there.

2. Results

2.1. Method of Analyses

[5] We perform a statistical and detailed examination of ELF/VLF electromagnetic waves in the dayside magnetosphere. There are ~1 1/2 years where the Polar Plasma Wave Instrument (PWI) was operational, from 1 April 1996 to 15 September 1997. All of the available data are used in this study.

[6] The data are taken from the Polar PWI [*Gurnett et al.*, 1995]. Specifically, we use the High Frequency Waveform Receiver (HFWR) 2 kHz bandwidth data.. The data set consists of full 3-axis magnetic and 3-axis electric waveform data obtained in ~0.45 s snapshots every ~127.8 s in the frequency range from ~20 Hz to ~2 kHz with a time resolution of ~224 μs. The data were processed in a manner similar to that used on the HFWR 25 kHz bandwidth data by *Santolík et al.* [2010a] to obtain a variety of plasma wave parameters, some of the most important being the spectral density of the Poynting flux, the polar angle θ_{PB0}, and the direction of the Poynting flux relative to the magnetic field, B_0. The electron plasma frequency was obtained from the Polar Sweep Frequency Receiver (SFR) spectral data. The latter is used to identify the plasmapause, if one exists. A detailed discussion of these parameters and their derivations can be found in *Santolík et al.* [2010a, 2010b].

[7] Single wave cycle (360° phase rotation) analyses and knowledge of the ambient magnetic field direction, B_0, were used to obtain the wave handedness, direction of propagation (relative to B_0) and ellipticity. The coherency of upcoming ELF waves at Polar altitudes will be shown and discussed.

[8] Multiple wave cycles and single wave cycles are analyzed by a minimum variance technique [*Sonnerup and Cahill*, 1967; *Smith and Tsurutani*, 1976]. In this method the magnetic field covariance is diagonalized identifying the maximum, intermediate and minimum variance directions. By standard notation, these will be called the B_1, B_2 and B_3 directions, respectively. The corresponding eigenvalues are denoted by λ_1, λ_2, and λ_3. The magnetic field wave data are rotated into this right-hand minimum variance coordinate system for detailed wave analyses. Pertinent information gained from this method are: 1) the B_3 direction is the direction of the wave phase velocity k direction (there is a 180° ambiguity in absolute direction that can be removed by use of the electric field components, as was done for the Poynting flux [*Santolík et al.*, 2010a]). Further discussion on why the use of the wave magnetic components is the most efficient way to determine k is given in *Verkhoglyadova et al.* [2010]. 2) parallel propagating and obliquely propagating waves can be distinguished once the direction of k relative to B_0 is known. This angle will be called θ_{kB0}. A plot of the B_1 and B_2 components with time (called a hodogram) give the polarization (circular, elliptical, linear) of the waves.

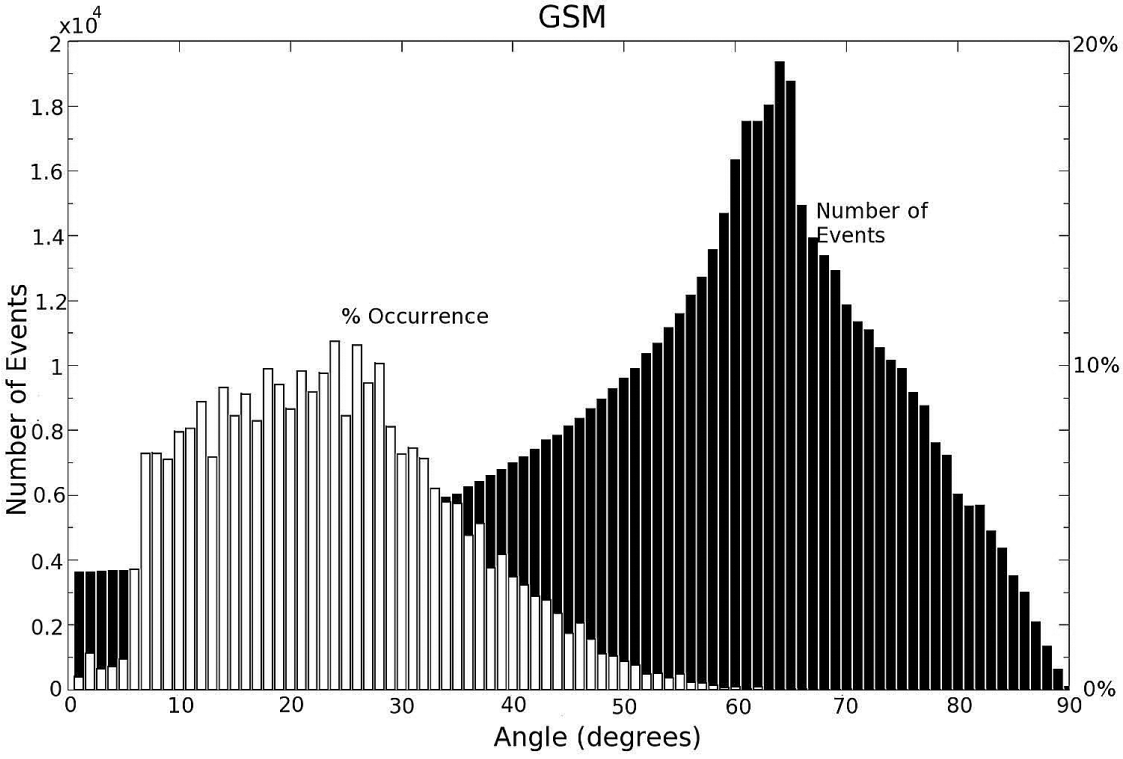

Figure 1. The wave percentage detection as a function of magnetic latitude (white) and the Polar satellite orbital coverage distribution (black). The scale of the former is given on the right and of the latter on the left.

The ratio λ_1/λ_2 can be used to determine a rough quantitative estimate of the polarization (this quantity is "rough" because total wave cycles are needed for accurate determinations). A λ_1/λ_2 value of 1.0 indicates circular polarization and infinity, linear polarization. Finally, 3) if the magnetic field B_0 direction is known relative to k, the sense of magnetic field rotation can be determined, identifying whether the wave is rotating in a right-hand (electron) sense or a left-hand (ion) sense. All of these various features identify the wave mode. This can be done from a single cycle of a wave. These details are needed for accurate wave-particle interaction modeling.

[9] Our study will focus on the dayside region of the magnetosphere. We have used L*, which is the McIlwain L parameter modified for solar wind pressure and interplanetary conditions [*Roederer*, 1970; *Santolík et al.*, 2010a] and magnetic local time (MLT) to bin the data for the statistical analysis portion of the paper. Electrostatic waves, when identified, were not used for the survey. We use a bin scale size of ΔL* = 1 and ΔMLT = 1 h for our unit spatial area. We analyze this space from L* = 2 to 9. For a wave "event," we use a time scale of 2 min and 7.8 s., the intrinsic rate of the HFWR data mode that was used.

[10] The intervals where waves were detected were almost solely in the northern hemisphere, with only ~1% detected in the southern hemisphere. The cause of this is because the satellite spent 99% of each orbital period in the northern hemisphere (this percentage changed after 1997). These events were included for completeness of the study.

[11] Figure 1 shows the percent occurrence of the electromagnetic wave detection as a function of magnetic latitude. This quantity is shown in white, with the scale on the right. The number of wave pass intervals are given in black, with the corresponding scale on the left. The figure shows that Polar covered primarily midlatitude ranges in the L* range of the study. Wave detection was likewise primarily limited to midlatitude values. Figure 1 is a modification of *Tsurutani et al.* [2011, Figure 3]. A sample orbit and the location of wave detection were also shown in *Tsurutani et al.* [2011] for the interested reader. We can make additional trajectory/wave detection information available to the interested reader.

2.2. Statistical Surveys of ELF/VLF EM Waves

[12] An average of the Poynting flux propagation angle was calculated for each frequency bin (there were 23 frequency bins) from 21.7 Hz to 1.79 kHz for each ΔL*-MLT spatial region. For each ~2 min interval that waves were detected, the Poynting flux angle was recorded. The average of angles for all the measurements taken for that bin was weighted by the logarithm of the wave intensity. Logarithms of the intensity were used because the wave intensity varied by orders of magnitude from one event to the next. All of the results from the 23 frequency bins are available upon request. In the following section, we will show a limited portion of the results, for ~360 Hz, ~800 Hz, ~1.2 kHz and ~1.8 kHz where there were significant findings. Other frequency ranges which had similar physical results (to those above) will not be displayed.

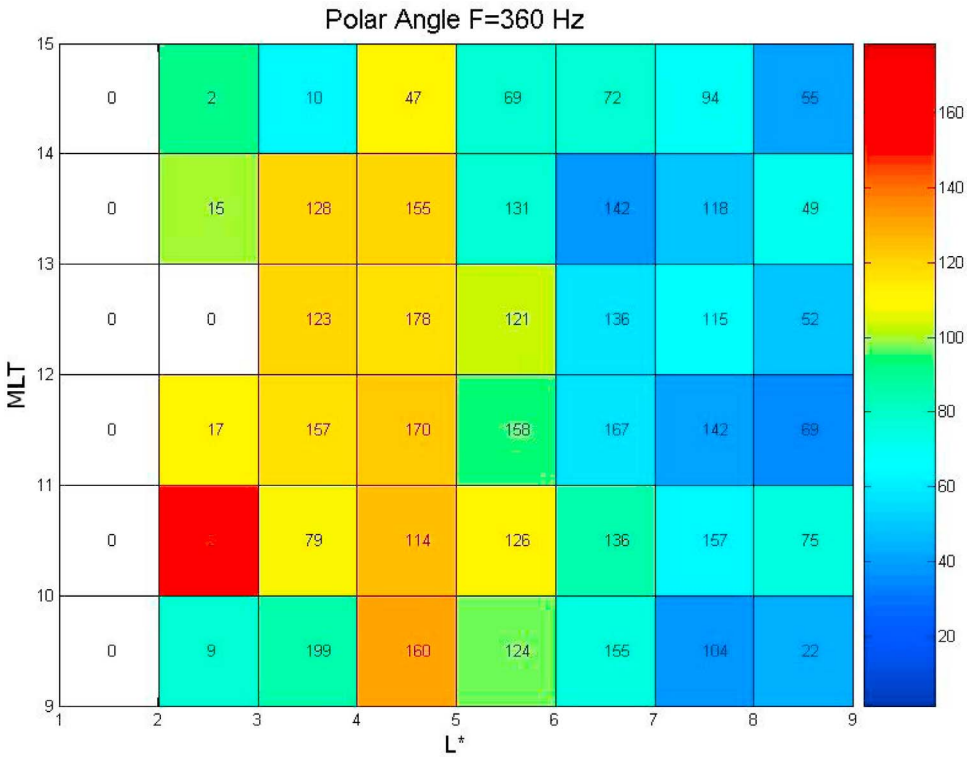

Figure 2. A distribution of wave Poynting vector polar angles as functions of MLT and L* for ~360 Hz waves. The blue color for the bins indicates downgoing waves and orange and red indicate upcoming waves. Each ~2 min event was weighted by its log of the wave intensity to form the average polarization for each bin (the color). The number of ~2 min events is indicated in each box.

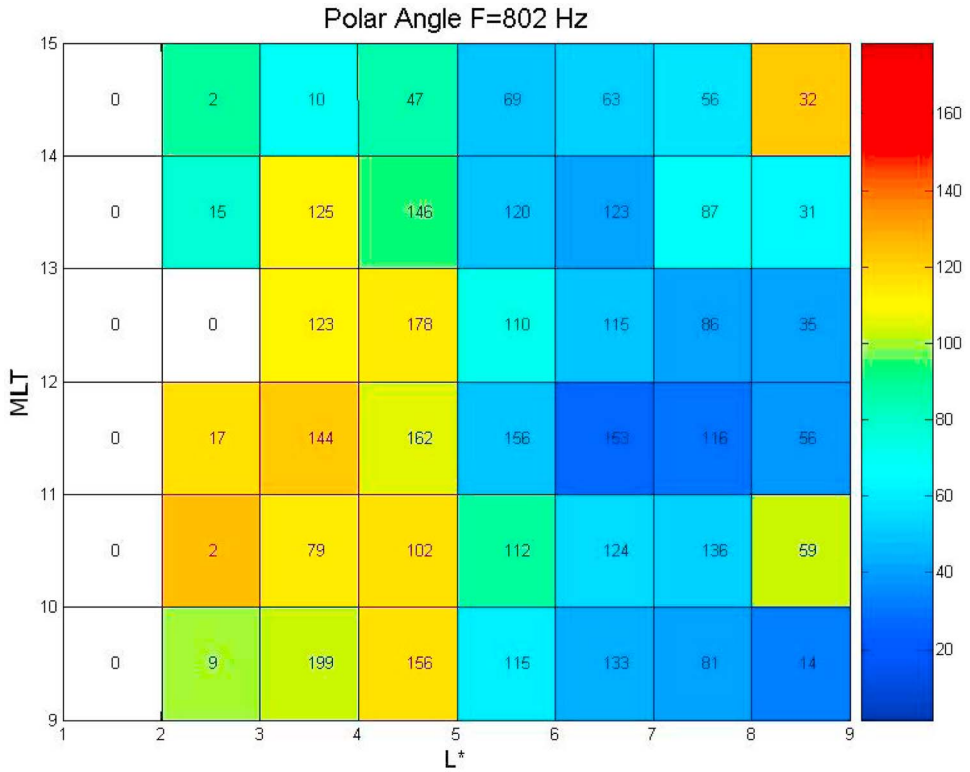

Figure 3. Same as for Figure 2, except for ~800 Hz waves.

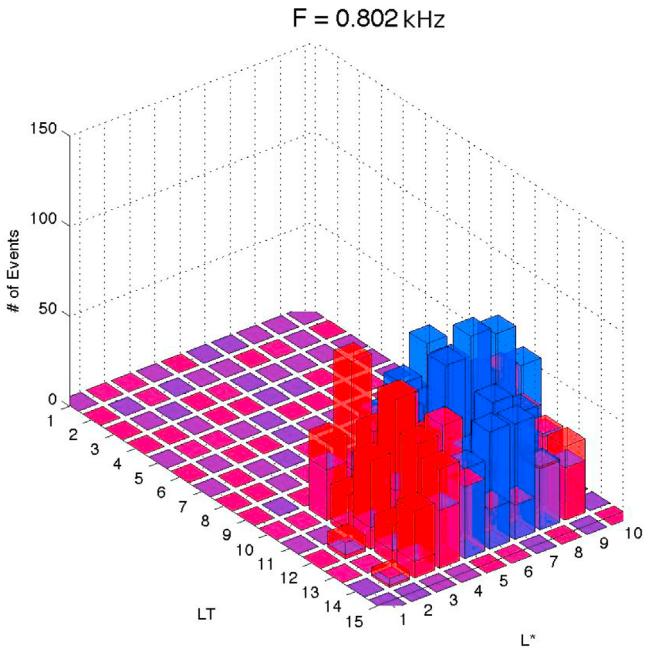

Figure 4. The distribution of ~800 Hz waves with Poynting vector angles within 30° of the ambient magnetic field displayed in histogram format. Blue (downgoing) waves have Poynting vector angles of 0° to 30° relative to B_0 and red (upgoing) waves have angles 150° to 180° relative to B_0. The vertical scale gives the number of events in each bin.

2.2.1. ~360 Hz Waves

[13] Figure 2 shows the results for the ~360 Hz frequency waves. The color scheme is shown in degrees in the legend on the right of the figure. Some comments should be made about the construction of the "color" in Figure 2. The color indicates the log-intensity-averaged direction of wave propagation, e.g., a blue color designates that on (intensity) average, the waves were propagating along the field lines downward toward Earth. It should be noted that there may have been lower intensity upward propagating (red) waves detected in that bin as well, but they were "intensity-dominated" by the downward propagating waves. Thus averaging of an intense downward wave with a less intense upward propagating wave interval, will result in a downward propagating average.

[14] What is noteworthy of the results in Figure 2 is that from L* = 6 to 9, the EM waves are primarily downward propagating (blue) and from L* = 3 to 5, the waves are upward or obliquely propagating (orange-brown). There is a thin intermediate strip near L* = 5 to 6 for which the waves are obliquely propagating (yellow or green). It should be noted, however, that a downgoing wave bin and an upcoming wave bin with equal intensity will average to an "oblique" wave. Thus the interpretation of this result is not straightforward. This topic will be discussed again later in the paper.

2.2.2. ~800 Hz Waves

[15] Figure 3 shows the Poynting vector polar angle distribution for ~800 Hz waves. The color again indicates the log-intensity-averaged direction of wave propagation, The downgoing waves (blue with some dark green) are in the outer regions of the magnetosphere from L* = 5 to 9 and the upcoming, oblique waves (yellow and orange-brown) are from L* = 2 to 5. There are also some light green colored bins as well. This band of upward obliquely propagating waves at ~800 Hz is at a lower L* range than for the ~360 Hz waves.

[16] A different viewpoint of the ~800 Hz waves is presented in Figure 4. The parallel/antiparallel (downward/upward) propagating waves are examined. The parallel waves are defined as those propagating within θ_{PB0} = 0° to 30° and antiparallel waves as those propagating within θ_{PB0} = 150° to 180°. The L* value in the figure corresponds to the right-hand edge of the bin and the MLT value to the left-hand edge of the bin. For each bin, the

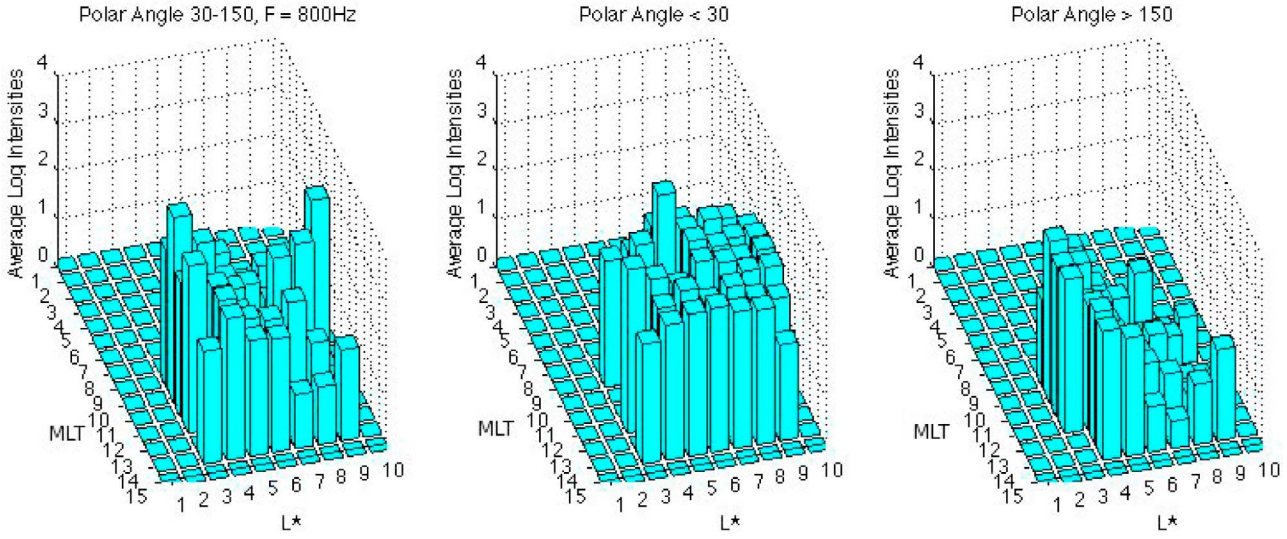

Figure 5. The spatial distribution of the log of the wave intensities for ~800 Hz waves. The log scale is given in the rear left of each panel. The scale has been shifted by 10^{-9} nT^2. (left) Oblique waves, (middle) parallel waves with θ_{PB0} < 30° and (right) waves with θ_{PB0} > 150°. Figures 5 (middle) and 5 (right) roughly correspond to blue and red waves, respectively.

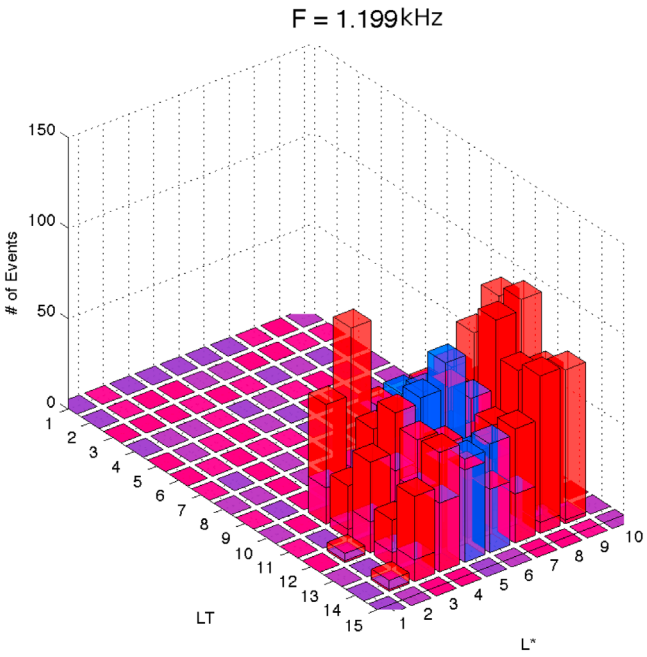

Figure 6. A distribution of ~1.2 kHz waves. The format is the same as Figure 4.

number of both θ_{PB0} = 0° to 30° (parallel) and θ_{PB0} = 150° to 180° (antiparallel) cases are indicate. The dominant (>50%) case is displayed on top.

[17] A predominance of upcoming (red) waves is noted from L* = 2 to 6 and downgoing (blue) waves are present from L* = 6 to 9. This is similar to the distributions of all ~800 Hz waves shown in Figure 3. There is a small set of upcoming (red) waves at L* = 8 to 9. This is particularly noticeable at MLT = 1300 to 1500.

[18] Figure 5 gives the average wave power of ~800 Hz waves over each ΔL*-ΔMLT bin. The results of this figure are complementary to those of Figure 4 (and different from Figure 3). The wave intensities of all wave events in each bin were first calculated, then the logarithms were averaged. Figure 5 (left) gives "oblique" waves with 30° < θ_{PB0} < 150°, Figure 5 (middle) gives "parallel" (downward) waves with 0° < θ_{PB0} < 30° and Figure 5 (right) gives "antiparallel" (upward) waves with 180° > θ_{PB0} > 150°. Note that all intensities have been shifted by 10^{-9} nT^2 for easier visualization. The number of events per bin are given in Appendix A for interested readers.

[19] Figure 5 (middle) indicates that the log intensity of the downgoing waves with 0° < θ_{PB0} < 30° is generally constant over L* and MLT, but slightly weaker at L* < 5 (this varies from bin to bin). Figure 5 (right) indicates that upcoming waves with 180° > θ_{PB0} > 150° have highest intensities both at low L* (3 to 6) and very high L* (8 to 9). The oblique waves (Figure 5, left) have highest intensities at low L* = 3 to 4 and at large L* = 8 to 9. The oblique waves are often more intense than even the downward 0° < θ_{PB0} < 30° waves. We note that the parallel and antiparallel wave categories, waves with θ_{PB0} < 30° and θ_{PB0} > 150°, respectively, roughly corresponds to the downward propagating (toward the Earth) blue waves and upward propagating red waves discussed earlier (Figure 3). The waves with θ_{PB0} < 30° have higher intensities at high L* than the waves with θ_{PB0} > 150° and the waves with θ_{PB0} > 150° have higher intensities at lower L* than the waves with θ_{PB0} < 30°, which is why the bars in Figure 4 are blue at high L* and red at low L*.

2.2.3. ~1.2 kHz Waves

[20] Figure 6 shows the distribution of parallel/antiparallel (downward/upward) propagating ~1.2 kHz waves. The upcoming (red) waves are present from L* = 2 to 5 and from L* = 6 or 7 to 9. The large L* upcoming wave region is now larger than that for ~800 Hz waves (Figure 4). The downgoing blue waves are now present only from L* = 5 to 6 or 7.

[21] Figure 7 is the same format as in Figure 3 but for ~1.2 kHz waves. The various panels give the average of the logarithm of the wave intensities for both oblique (Figure 7, left) and parallel/antiparallel (Figures 7 (middle) and 7 (right)) propagating waves. The most intense waves, shown in Figure 7 (middle), are propagating downward (θ_{PB0} < 30°). This is true for all L* even those inside L* = 6.

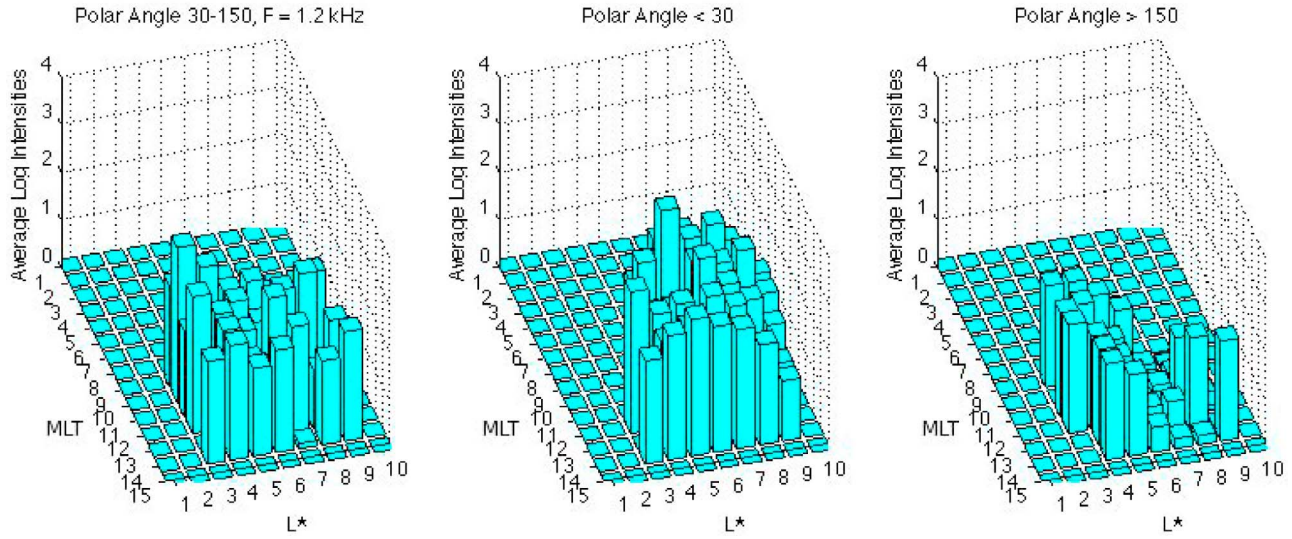

Figure 7. Same format as Figure 5, except for ~1.2 kHz waves.

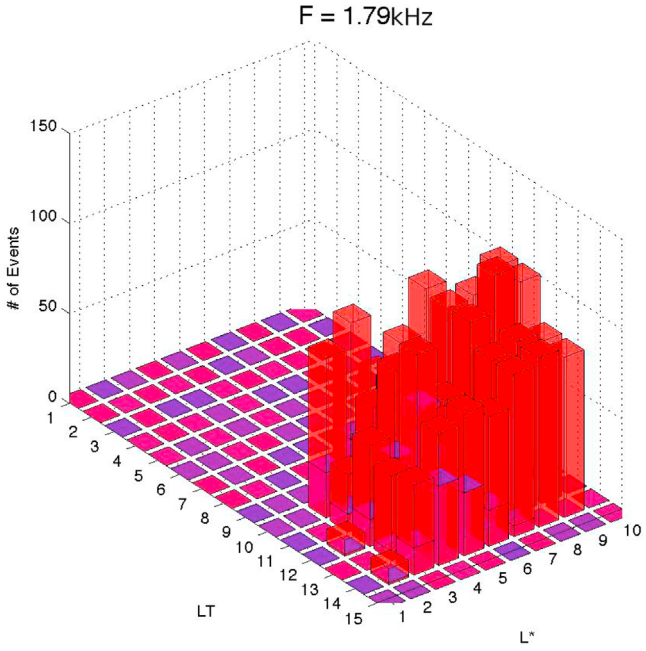

Figure 8. The same format as in Figure 4 but for ~1.8 kHz.

Upward propagating waves ($\theta_{PB0} > 150°$) are detected at low L* (L* = 3 to 6) and at high L* (L* = 8 to 9) with one to two orders of magnitude less intensity.

[22] The oblique waves are intense and are distributed without any particular weighting in L* and MLT. The most intense wave averages are found from L* = 3 to 4.

[23] Statistical information about the events for the ~1.2 kHz waves are given in Appendix A. The statistics of ~1.8 kHz waves are discussed there as well.

2.2.4. f > 1.8 kHz Waves

[24] Figure 8 displays the parallel and antiparallel (downward and upward) propagating ~1.8 kHz waves. The histogram shows that almost all waves are upcoming (from below the spacecraft).

[25] Figure 9 shows the average intensities of the parallel and antiparallel ~1.8 kHz EM waves. The distribution is similar to the ~1.2 kHz waves. The most intense waves are downgoing (blue) waves (Figure 9, middle). They are located almost equally in L*-MLT space. The oblique waves are slightly lower in intensity and are distributed uniformly as was the case in Figure 7. There is a small amount of intense waves that are propagating upwards.

2.3. Case Study of EM Waves

[26] The previous section gave statistical results of dayside electromagnetic waves. In the following section we will show results from a single satellite pass. These higher time resolution results are shown to provide context to the statistical results. The minimum variance analyses on these data will give the wave k vector direction relative to the ambient magnetic field (θ_{kB}), details of the wave ellipticity, wave coherency and the degree of plane polarization. These values will be far more accurate than those of the Poynting vector analyses shown earlier. However, the general spatial and frequency dependence was best shown by the Poynting flux statistical survey. It also should be noted by the reader that the wave k direction is different than the Poynting flux direction. The first is useful for understanding wave-particle interactions and the latter gives energy flow directions. The two parts of the study, the statistical part and the case study part are complementary to each other.

[27] In Figure 10, the panels from top to bottom contain the following: the sum of the three magnetic power spectra (autopower spectra), sum of the three electric power spectra, spectral density of the Poynting flux, the electron plasma frequency, the Polar angle (θ_{PB0}) of the Poynting flux relative to B_0, the polar and azimuthal (φ) angles, the polarization ellipticity, and the degree of planar polarization of the waves for a Polar (outbound) pass on 29 May 1996. The local time of the event is ~9.6 MLT. The interval starts at ~0130 UT where L* = 4.4. In the fifth panel, it can be noted that the upcoming (red) waves extend from ~0130 to 0147 UT, and at ~0147 UT (L* ~ 5.7) the wave direction sharply changes from upcoming to downgoing.

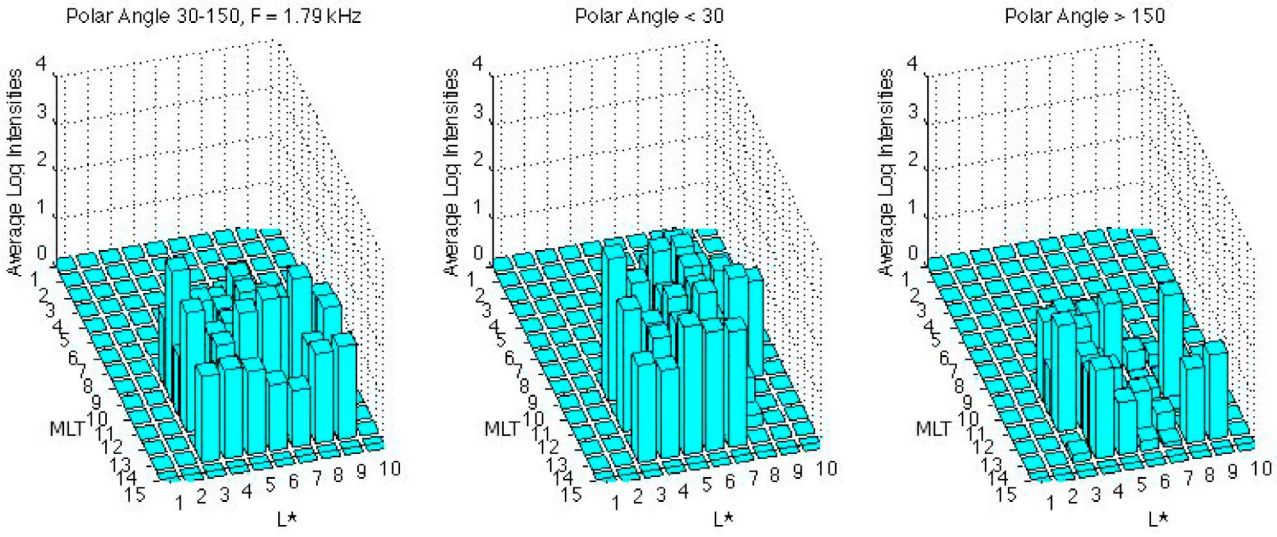

Figure 9. Same format as Figure 5, except for ~1.8 kHz waves.

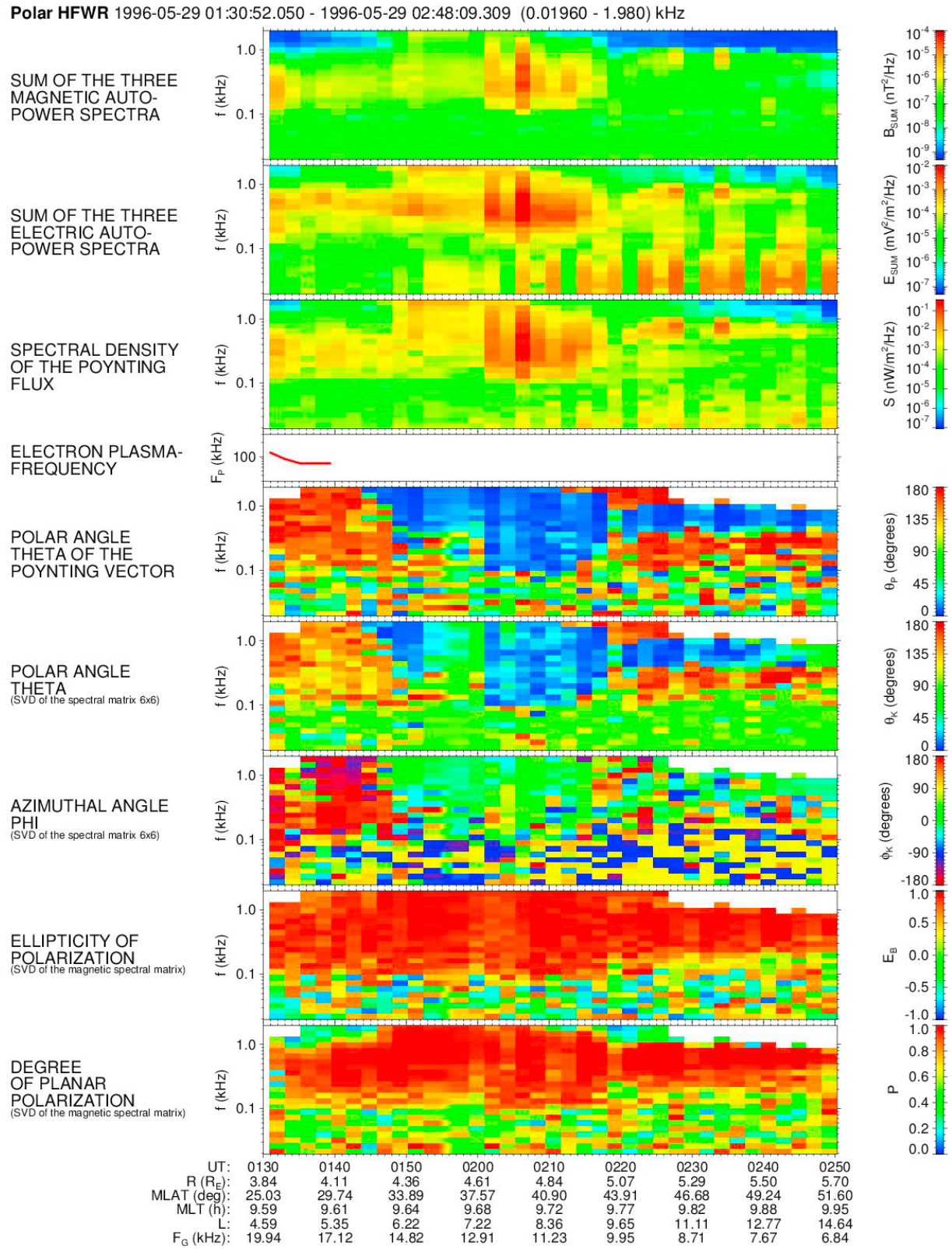

Figure 10. Upcoming (red) waves are present prior to 0146 UT. Downgoing (blue) waves are present beyond this time. Upcoming waves were detected on L* = 4.4 to 5.7 field lines and downgoing waves from L* = 5.7 to 8.5. The event occurred on 29 May 1996 at ~9.7 MLT.

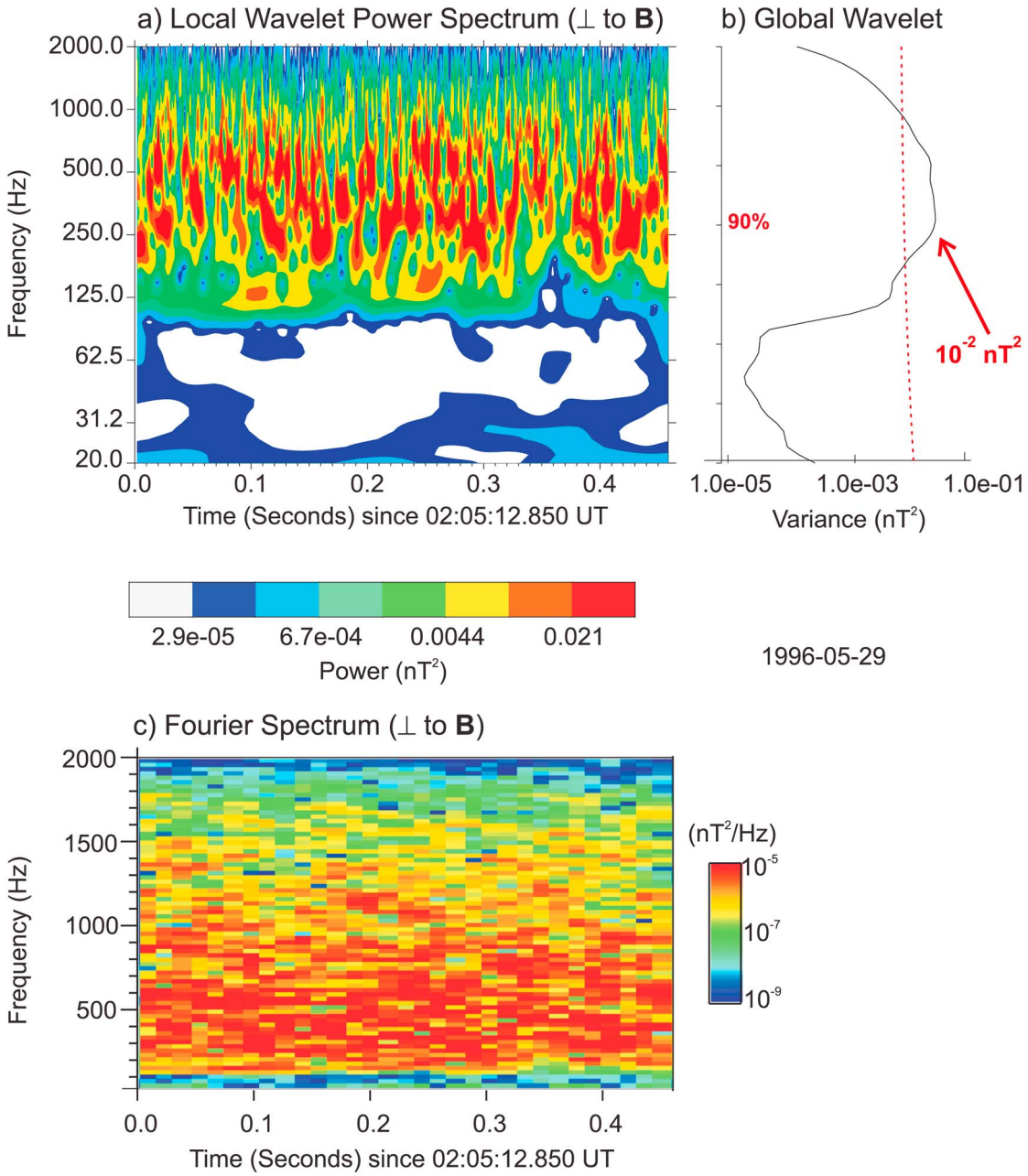

Figure 11. (a) A wavelet analysis, (b) a global wavelet analysis, and (c) a Fourier spectrum for a 0.45 s interval of downward propagating chorus starting at 0205.12.8 UT May 29, 1996.

At ~0230 UT near the maximum intensity of the downgoing (blue) waves, the spacecraft was located at L* = 8.5. These downgoing waves were detected in the outer magnetosphere. Chorus is confined primarily to this region of the magnetosphere, so it is presumed that these waves are chorus.

[28] The figure shows the general relationship between downgoing (blue) waves and upgoing (red) waves as was observed from our visual examination of the SFR plots prior to the statistical analyses. There is a data gap in the plasma frequency at the time of the switch between upcoming and downgoing waves, ~0146 UT. However, from an examination of the plasma frequency at other times on this pass when data were available, the authors have concluded that there was probably no sharp density gradient present, i.e., there was no obvious plasmapause as we know it, for this crossing.

[29] Figure 11 shows a wavelet analysis (Figure 11a), a global wavelet analysis (Figure 11b) and a Fourier spectrum (Figure 11c) of a ~0.45 s interval of the downgoing (blue) waves at ~0205 UT 29 May 1996. All three analyses were performed on the magnetic component perpendicular to B_0 (a wave transverse component). The global wavelet spectrum is a measurement of the time-average wavelet spectrum over all the local wavelet spectra for the entire interval and is an efficient estimator of the true power spectrum, thus providing the variance of power over frequency. The red-dashed line provides the 90% confidence level, using a chi-square distribution, when compared to a Fourier power spectrum

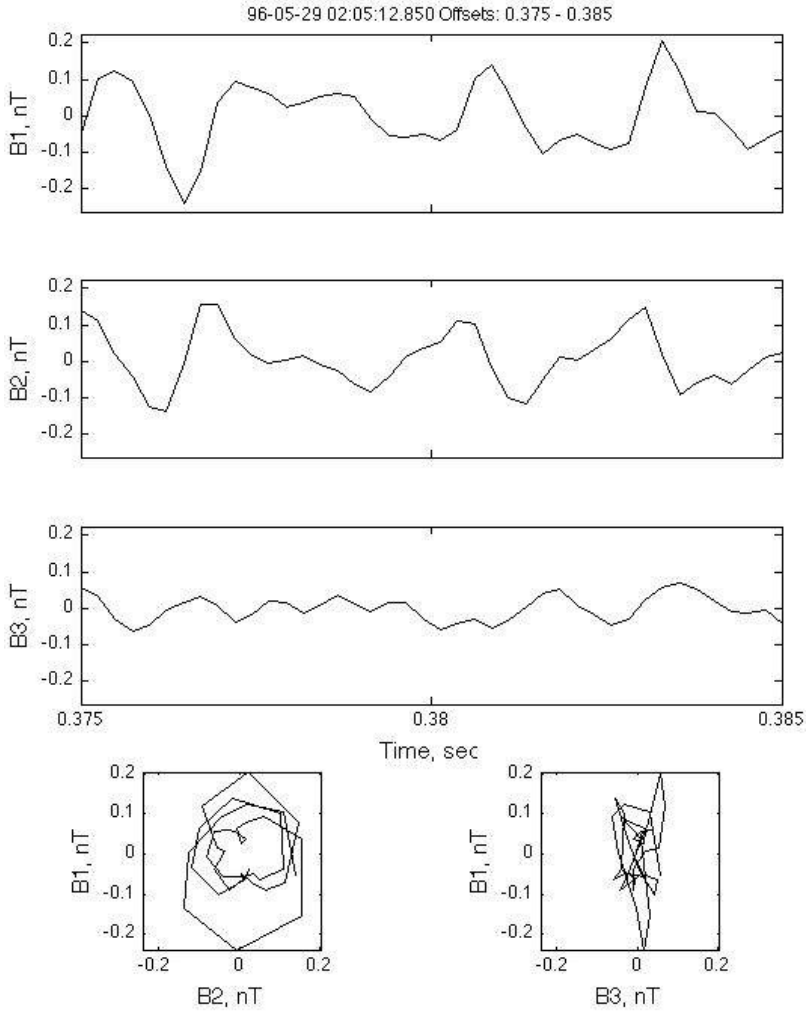

Figure 12. An example of phase-steepened chorus and coherence over several cycles.

(white noise) at each scale (frequency). A peak in the global wavelet variance which lies significantly to the right of the red dashed line (larger variance) thus can be assumed to be a true feature with 90% confidence.

[30] These downgoing (blue) waves are noted to generally lack coherence (Figure 11a) with a peak power spectral density of $\sim 10^{-2}$ nT^2 (Figure 11b). These chorus emissions have a structureless nature over a broad frequency range extending from ~100 Hz to ~1.5 kHz (Figure 11c). There are no rising tone elements as found near the equatorial generation region [*Burtis and Helliwell*, 1969; *Tsurutani and Smith*, 1974]. For more information on the wavelet analysis carried out here, the reader is referred to *Tsurutani et al.* [2011, section 3.2].

[31] Details of the waves in the Figure 11 interval were determined using high-resolution, three-component magnetic field data by the application of minimum variance analyses [*Sonnerup and Cahill*, 1967; *Smith and Tsurutani*, 1976]. The results are summarized here to conserve space. In general the waves were found to be right-hand circularly polarized and planar. The wave phase direction of propagation k relative to B_0, θ_{kB0}, was field-aligned or slightly oblique to B_0. The waves were not coherent over long intervals of time. There were no chorus element and subelement structures noted. The waves are typically coherent over one or two cycles at most. The above downgoing outer zone chorus properties are essentially the same as those discussed previously for Polar wave measurements in *Tsurutani et al.* [2011].

[32] The above results are in sharp contrast to chorus properties in the equatorial (or minimum B) generation region [*Tsurutani and Smith*, 1974, 1977; *Anderson and Maeda*, 1977; *LeDocq et al.*, 1998; *Lauben et al.*, 2002; *Verkhoglyadova et al.*, 2009; *Tsurutani et al.*, 2009]. At the equator, the chorus elements (~0.5 s) consist of shorter duration subelements or packets lasting 10 to 100 msec [*Santolík et al.*, 2004b; *Verkhoglyadova et al.*, 2009; *Tsurutani et al.*, 2009]. The wave transverse components (B_1 and B_2) remain in phase for many cycles [see *Tsurutani et al.*, 2011].

[33] There were some chorus waves identified in the Figure 11 interval that had unique properties that have not been identified before. Figure 12 shows one such example. In the figure, the top three panels are the magnetic field components in the maximum (B_1), intermediate (B_2) and minimum (B_3) variance directions. The bottom two panels are the B_1-B_2 and B_1-B_3 hodograms. The former hodogram gives the polarization of the waves and the latter hodogram gives the degree of planarity of the waves. The example given shows multiple cycles of a wave that is not sinusoidal. One edge of the wave is steepened in phase. This same

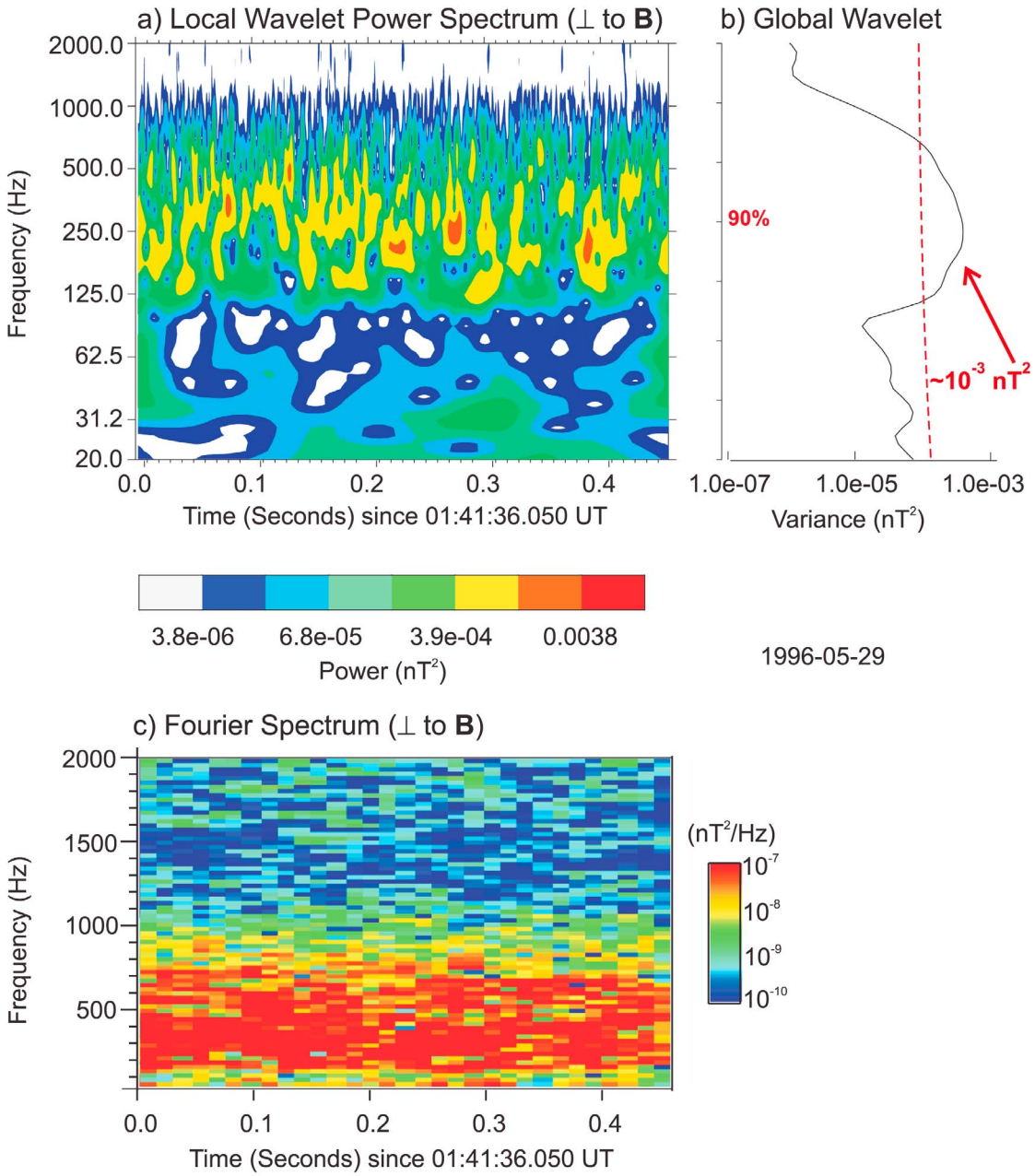

Figure 13. Same format as in Figure 11. An example of the upward (red) propagating waves at ~0141 UT in Figure 10.

feature has been noted in right-hand polarized cometary (magnetosonic) waves [*Tsurutani et al.*, 1987]. The θ_{kB0} angle is ~24°. λ_1/λ_2 is ~1.8. The wave amplitude is ~±0.15 nT, quite large for chorus [*Tsurutani and Smith*, 1977; *Tsurutani et al.*, 2009; *Verkhoglyadova et al.*, 2009]. The large wave amplitude and slightly oblique propagation may lead to the wave phase steepening.

[34] Figure 13 gives the wavelet power spectra, global wavelet power and Fourier spectrum for a portion of the upward propagating waves. The interval analyzed is 0.45 s starting at 0141:36 UT 29 May 1996. The format is the same as in Figure 11 for the downward propagating waves. The power of the upward propagating (red) waves for the event in Figure 13 is ~10^{-3} nT^2 or an order of magnitude lower than the downward propagating (blue) waves in Figure 11. The Fourier spectrum (Figure 11c) shows that the emission is structureless and broadbanded extending from ~100 to ~900 Hz. These wave properties are similar to that known for plasmaspheric hiss. The local magnetic field magnitude B_0 is ~595 nT and $f_{ce}/2$ is 16.6 kHz. These waves were detected at a magnetic latitude of −22°. The possible source of these waves will be discussed in the next section.

[35] Figure 14 displays the three components of the wave magnetic field data in minimum variance coordinates for the Figure 13 event. The waves are generally structureless. The B_1 component is the largest, with the B_2 component slightly smaller. The left-hand B_1-B_2 hodogram is in agreement with this identification. The waves are thus slightly

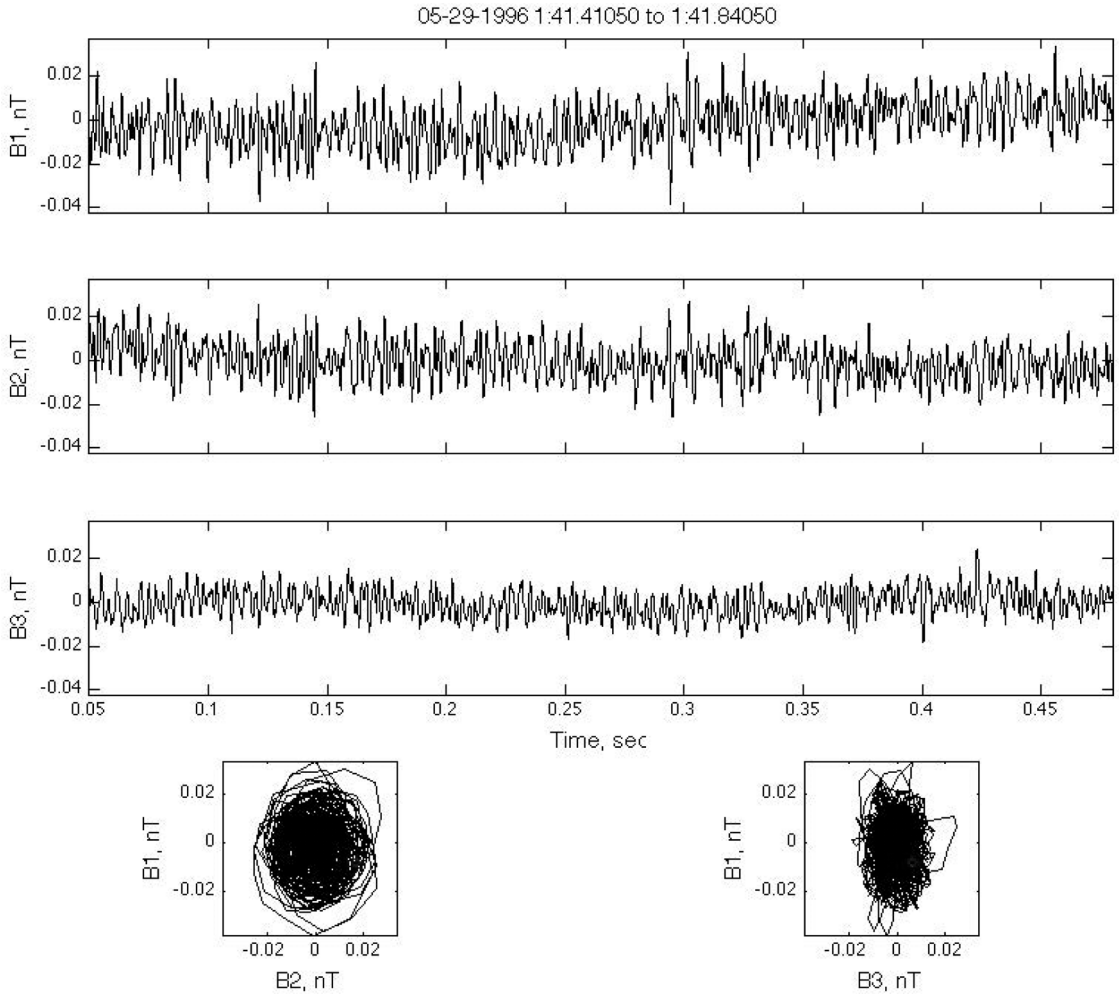

Figure 14. A portion of the waveform data of Figure 13. These are downgoing (red) waves. The waves are slightly elliptically polarized.

elliptically polarized with $\lambda_1/\lambda_2 = 1.3$. The average angle of propagation θ_{kB0} is ~18.0°. The coherency of the waves lasts for 1 or 2 cycles, at best. Examples of single cycles exist near 0.3 s. Examples of multiple cycles can be found at ~0.08 s and ~0.025 s.

[36] A single cycle of the waves is shown in Figure 15. The format is the same as in Figure 12. The time of the event is 0141:36.509 UT. In the hodogram at the bottom left, the wave starts at the diamond, B_0 is out of the paper, and thus the wave is right-hand polarized. The angle of propagation θ_{kB0} is ~19°. From the B_1-B_2 hodogram, it is clearly noted that this wave is elliptically polarized. The ratio λ_1/λ_2 had a value of 1.8. It should be noted that this is different from the downward propagating chorus which are circularly polarized and propagating nearly parallel to B_0 noted in *Tsurutani et al.* [2011]. Cold plasma theory [*Verkhoglyadova et al.*, 2010] cannot explain this noncircular polarization. Warm plasma theory will be necessary. Such waves will have to be treated differently by wave-particle modelers.

3. Summary and Discussion

[37] A statistical survey of ELF/VLF electromagnetic waves has been performed on Polar plasma wave data to obtain information of wave occurrence frequencies, intensities and directions of propagation that will be useful for wave-particle interaction studies and modeling. We have focused on the dayside 09 to 15 MLT region from L* = 2 to 9 during a time of solar minimum (1996–1997).

3.1. Where Is the Plasmasphere and Does This Order the Wave Data?

[38] A naturally occurring thermal plasma region that may order the data of downgoing and upcoming low frequency waves is the plasmasphere, a region of high density thermal plasma, typically extending from the Earth out to L ~ 6 during quiet periods [*Carpenter*, 1963, 1966]. Chorus is typically detected outside the plasmasphere in the outer region of the magnetosphere, and plasmaspheric hiss, as the name implies, primarily inside the plasmasphere.

[39] The outer boundary of the plasmasphere, or plasmapause, is noted to be dependent on geomagnetic activity [*Chappell et al.*, 1970, 1971; *Carpenter and Anderson*, 1992; *Sheeley et al.*, 2001; *Moldwin et al.*, 2002; *O'Brien and Moldwin*, 2003]. In the nightside region of the plasmasphere, strong storm-time convection electric fields erode away the plasma, moving the plasmapause inward [*Ridley*

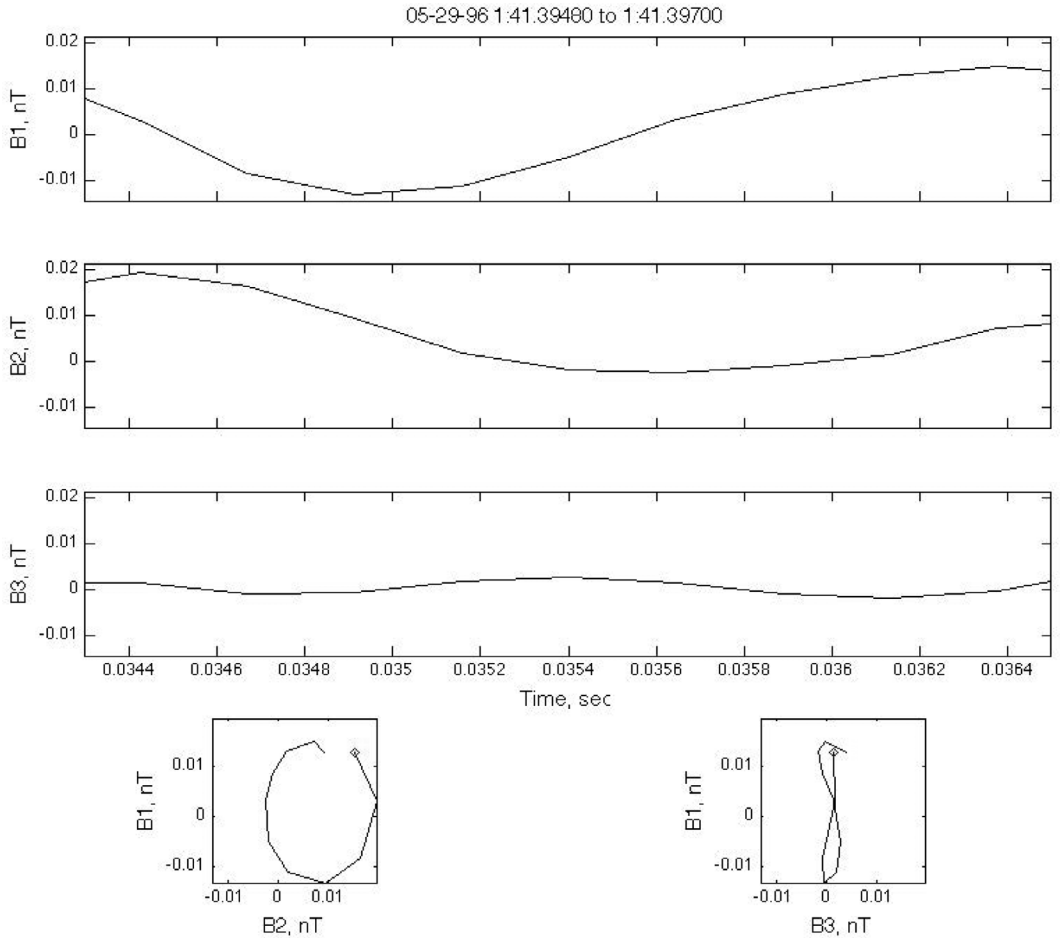

Figure 15. One cycle of the waves from the interval in Figure 13. The coordinate system is right-handed and the wave interval starts at the diamond. The wave is right-hand elliptically polarized.

and Liemohn, 2002]. However, on the dayside, the same convection electric fields cause the formation of high density plasma "tails" or "plumes" [*Grebowsky*, 1970; *Chappell*, 1974] that are convected sunward to the magnetopause. Thus on the dayside, there is often no obvious plasmapause at all (J. Goldstein, personal communication, 2011).

[40] The Polar plasma wave data were not always useful in identifying where the spacecraft was relative to the plasmasphere (as noted in Figure 10, the plasma density was often not always available due to the occasional lack of the presence of upper hybrid waves). For this reason, we use geomagnetic activity to identify the nominal location of the plasmapause to apply to the study's statistical results. We use the *O'Brien and Moldwin* [2003] empirical model for the location of the plasmapause, L_{pp}, based on the Dst index (the authors argue that the Dst index is superior to models based on the Kp index):

$$L_{pp} = aQ + b$$

where $Q = \log_{10} |\min_{-24,0} Dst|$, and a and b are empirically derived constants given in *O'Brien and Moldwin* [2003, Table 2]. The average Dst value during chorus detection, taken from *Tsurutani et al.* [2011], is −12.1 nT with a standard deviation of 14.7 nT. Thus the *O'Brien and Moldwin* [2003] empirical relationship indicates that the plasmapause, when it exists, should be at about L = 4.6 with a range from 4.1 to 6.3. In the following discussion, we will assume that waves detected outside of 4.6 Re are outer zone chorus emissions which have propagated from the equatorial or minimum B pockets to the Polar location. (We note that O'Brien and Moldwin have based their empirical model on the L parameter, where we have used L* throughout this paper. At low L or L* values, the difference is almost negligible. For example in Figure 10, the L* value of 5.7 was a L value of 5.85.)

[41] It is found that downward propagating waves (presumably chorus) are observed primarily outside of the average location of the plasmapause in the outer region of the magnetosphere (Figures 2 and 3). *Tsurutani et al.* [2011] showed that this chorus is semi-coherent and structureless, in sharp contrast to ∼0.5 s coherent rising-tone structures detected in the generation region. The higher the frequency of the waves analyzed in the survey, the lower the L* location of detection. Figures 2 and 3 show the log of the Poynting vector flux. Figures 4 and 6 show the frequency of occurrence for downgoing and upcoming events. The results for Figures 2 and 3 are quite similar to those of Figures 4 and 6. This is expected since chorus is primarily

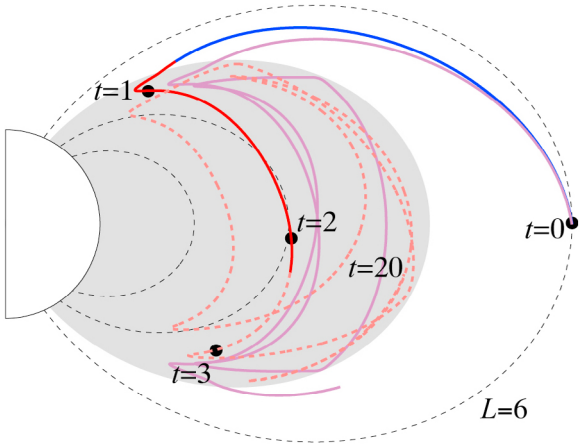

Figure 16. A model of chorus entry into the plasmasphere at low altitudes plus propagation and internal reflections.

generated between 0.25 f_{ce} < f < 0.75 f_{ce} at the local magnetic equator [*Tsurutani and Smith*, 1974, 1977; *Burtis and Helliwell*, 1976; *Anderson and Maeda*, 1977; *LeDocq et al.*, 1998; *Lauben et al.*, 2002; *Verkhoglyadova et al.*, 2009]. Higher frequency chorus will thus be generated at lower L* (and then propagate downward to the Polar spacecraft altitudes).

[42] The upcoming ~360 and ~800 Hz waves are detected primarily inside the average location of the plasmapause. The location of these waves (Figures 2 and 3) and their structureless nature (Figure 13c) leads us to presume that they are plasmaspheric hiss. These waves are about an order of magnitude lower in intensity than the downgoing chorus. The plasmaspheric hiss waves are semicoherent in nature (Figures 13–15), e.g., individual wave cycles are present, but multiple in-phase wave cycles (such as those for chorus in the generation region) are rare. For some cases, plasmaspheric hiss is elliptically polarized (Figures 14 and 15). *Lakhina et al.* [2010] gave an expression for pitch angle "transport" for coherent chorus "subelements" detected in the wave generation region. *Kennel and Petschek* [1966] assumed essentially incoherent waves. As was shown here and in *Tsurutani et al.* [2011], chorus detected away from the generation region is quasi-coherent. Perhaps a greater distance of wave propagation leads to a lower wave coherency. Thus, for accurate wave-particle interaction modeling, the wave coherency as a function of location should be modeled and then a new theory of a pitch angle diffusion developed. The new theory should give diffusion rate coefficients between those of *Kennel and Petschek* [1966] and *Lakhina et al.* [2010].

[43] There are intervals where it appears that there are waves with oblique directions of propagation (Figure 2, L* = 5 to 6 and Figure 3, L* = 4 to 5). They are localized in the region near the average location of the plasmapause. These waves are either obliquely propagating hiss or magnetosonic waves. Another possibility is that these oblique waves are simply an artifact of a summation of downward and upward propagating waves. However, we think that this is unlikely because the downward propagating waves are far more intense than upward propagating waves, which would give a downward average. Also in Figure 5 it was shown that at times the oblique waves could be even more intense than downward propagating waves. *Bortnik et al.* [2011] in a statistical wave-tracing analysis, indicated that obliquely propagating hiss would pileup near the plasmapause, a result consistent with the present observations. Further analyses will be necessary to determine whether this is the case or not. This is beyond the scope of this present paper.

[44] A detailed examination of one case was carried out where downgoing waves were detected in the range L* = 5.7 to 8.5 and upcoming waves were detected from L* = 4.4 to 5.7 (Figure 10). In this case the L* value of 4.4 had a L value of 4.65 and the L* value of 5.7 had a L value of 5.85. The waves were generally structureless. Where was the plasmapause during this event? The Dst value was positive for the whole day indicating a high solar wind ram pressure. Dst was +1 nT during hour 0, increased to +17 and +19 nT for hours 1 and 2, respectively. Dst was positive throughout the rest of the day. On closer inspection it was found that a high density heliospheric plasma sheet, HPS [*Winterhalter et al.*, 1994], associated with a heliospheric current sheet, HCS [*Smith et al.*, 1978] in the slow solar wind occurred during the time of interest. The HPS/HCS was followed by a high speed solar wind stream. The HPS started at ~0000 UT with a density of ~20 cm^{-3}, and gradually increased to ~40 cm^{-3} by 0250 UT, the end of our wave interval. This high density HPS compressed the magnetosphere leading to the positive SYMH values (SYMH is the average H component of near-equatorial magnetograms, taken at high time resolution). This data is not shown to conserve space, but can be made available for an interested reader. This is the standard sequence for high speed stream magnetic storms [*Tsurutani et al.*, 2006a, 2006b]. At the time of the HPS impingement, Polar was at ~9.7 MLT, so the compression effect would not be as great as if the spacecraft was at local noon. However, we note that the L* value is higher than L due to the solar wind compression effects. The O'Brien and Moldwin expression yielded a plasmapause location of L_{pp} = 6.3, if such a plasmapause existed during this time.

3.2. Possible Explanation of Upcoming ~360 and ~800 Hz Waves at Low L*

[45] A likely scenario that may explain part of our observations is based on the results from raytracing models [*Chum and Santolík*, 2005; *Bortnik et al.*, 2009a, 2009b; *Chen et al.*, 2009]. Figure 16 shows a variation of the *Bortnik et al.* [2009a] model, courtesy of J. Bortnik, 2012. Chorus emissions are generated at t = 0 at the equatorial plane and propagate inward in L* to low altitudes. At the encounter with the plasmapause (point 1) part of the waves is refracted into the plasmasphere. The chorus which is now inside the plasmasphere can bounce many times due to internal reflections, filling the plasmasphere with hiss-like ELF wave turbulence.

[46] It should be noted that the observation of waves predominately propagating in the upward direction from L* = 3 to 6 is not necessarily contradictory to the multiple wave reflections in the *Bortnik et al.* [2008, 2009a, 2009b] raytracing modeling. Since our statistical wave analysis was based on wave log intensities, this just implies that the most intense plasmaspheric waves have this upward directionality (at Polar altitudes). Waves that have been reflected within

the plasmasphere once or several times more may be present, but will be of lower intensity and tertiary in importance for wave-particle interactions, as one might expect.

[47] How would the *Bortnik et al.* [2008] picture be modified if there were no sharp plasmapause boundary, but only a gradual plasma density gradient out to the magnetopause? One would suspect that the same basic principle would apply, that wave refraction would occur and upward propagating chorus would be created at the crossover point. *Wang et al.* [2011] have commented on this very point. It might be easier to get chorus across a gradual density region such as a plasmapause boundary layer [*Carpenter and Lemaire*, 1997] than a sharp density gradient. *Chen et al.* [2012] and J. Bortnik (personal communication, 2012) have affirmed that chorus can indeed enter the plasmasphere when the plasmaspheric density gradient is gradual.

[48] Why are the intense ∼1.2 and ∼1.8 kHz waves at low L* downgoing at Polar, unlike lower frequency waves? Is this in contradiction with the Bortnik et al. model? These higher frequency chorus waves are expected to be generated at lower L* regions. Additionally they may occur during strong geomagnetic activity intervals when convection electric fields move the plasmapause inward. Thus the wave entry points across the plasmapause will be different than those for lower frequency waves. The lack of past observations of high frequency hiss (∼1.2 to 1.8 kHz) inside the plasmapause indicates that although these waves may enter the plasmasphere (from the present observations), the waves may be rapidly damped, not further amplified, or may propagate into lower L* regions where it is not detected by Polar. *Bortnik et al.* [2011] have suggested the last possibility.

3.3. Upcoming Waves at Large L* and f > 1.2 kHz

[49] In our statistical survey upcoming waves were detected at large L* for f = 800 Hz and ∼1.2 kHz waves (Figures 4, 6, and 7). Similar results were noted by *Santolík et al.* [2010a] for a different Polar wave data set. The source of these waves is unknown at this time. One possibility is these are chorus emissions that refracted to higher L* values. As chorus propagates from the equatorial generation region toward the Earth, reflection at the lower hybrid resonance (LHR) frequency [*Thorne and Kennel*, 1967] plus propagation back away from the Earth could be an explanation for these high L* waves. Another possible source is that the waves are reflected at the plasmapause back into the magnetosphere. Backward raytracing analyses such as those by *Chum et al.* [2005] and *Santolík et al.* [2006] may be the best way to provide answers to this question.

3.4. Upward Propagating Waves at f ∼ 1.8 kHz

[50] At even higher frequencies, f = 1.8 kHz, most of the wave events are propagating upward (Figure 8). However, when examined by wave intensity (Figure 9) it is found that the most intense waves are a mixture of downgoing and oblique waves. How can one reconcile these two observations? The obvious answer is that there are many upcoming wave events, but they are typically of low intensity. At this time the source of these waves is unknown. Two possibilities mentioned in the literature are lightning-generated sferics [*Kimura*, 1966; *Edgar*, 1976; *Parrot*, 1990] and power line harmonics [*Bell et al.*, 1982; *Koons et al.*, 1978; *Němec et al.*, 2006b].

4. Conclusions

[51] This dayside ELF wave survey shows that waves can be nicely sorted out by Poynting vector properties. The downward parallel propagating waves are outer zone chorus. The upward propagating ∼360 to ∼800 Hz waves inside the plasmasphere are probably plasmaspheric hiss. The plasmaspheric hiss is an order of magnitude less intense than downward propagating chorus, is quasicoherent in nature and is therefore secondary in importance for wave-particle interactions.

[52] The slightly elliptical polarization and the slightly oblique propagation of the hiss noted in the case study are interesting and new features. At this time, it is unclear how often this occurs. Both will be important for wave-particle interaction modeling.

[53] The intense, obliquely propagating waves inside the statistical location of the plasmapause (Figures 5 and 7) are a mystery. They may be hiss that have "piled up" just inside of the plasmapause that *Thorne et al.* [1979], *Bortnik et al.* [2011], and *Chen et al.* [2012] postulated through raytracing analyses. Further analyses will be required to confirm this.

[54] An example of a phase-steepened chorus wave (Figure 12) was shown for the first time. Similar waves have been detected in planetary foreshocks [*Tsurutani et al.*, 1993] and at comets [*Tsurutani et al.*, 1987] but at much lower frequencies (tens of mHz). These latter waves were on the MHD magnetosonic branch, the same as whistler mode waves studied here. At this time, it is unclear how often such phase-steepened chorus occurs. However, it should be noted that wave-particle interactions with phase-steepened and compressive waves will be considerably different than simple pitch angle scattering from cyclotron resonance with circularly polarized waves.

[55] It is noted that the plasmaspheric hiss (Figures 10 and 13–15) appears to be quite similar to the outer zone reflected chorus shown in *Tsurutani et al.* [2011]. This may be a possible explanation why hiss is sometimes detected in the outer magnetosphere [see *Tsurutani and Smith*, 1974, Figures 1–3] and why in this case it is so similar to plasmaspheric hiss (also reflected chorus).

[56] A final comment is that this survey was made for plasma wave data taken during a solar minimum interval. The average Dst value was −12.1 nT when waves were detected, and −9.8 nT during the Polar interval. The conditions for dayside ambient plasma (plasmasphere, boundary layers and tails) might be quite different than during solar maximum periods. A cautionary note to the reader is that the wave intensities and locations might be substantially different during another phase of the solar cycle.

Appendix A

[57] Figure A1 displays the ∼1.2 kHz wave average log intensities for $30° < \theta_{PB0} < 150°$ (Figure A1, left), $0° < \theta_{PB0} < 30°$ (Figure A1, middle), and $150° < \theta_{PB0} < 180°$ (Figure A1, right). This figure is similar to Figure 6, but is shown in a flat

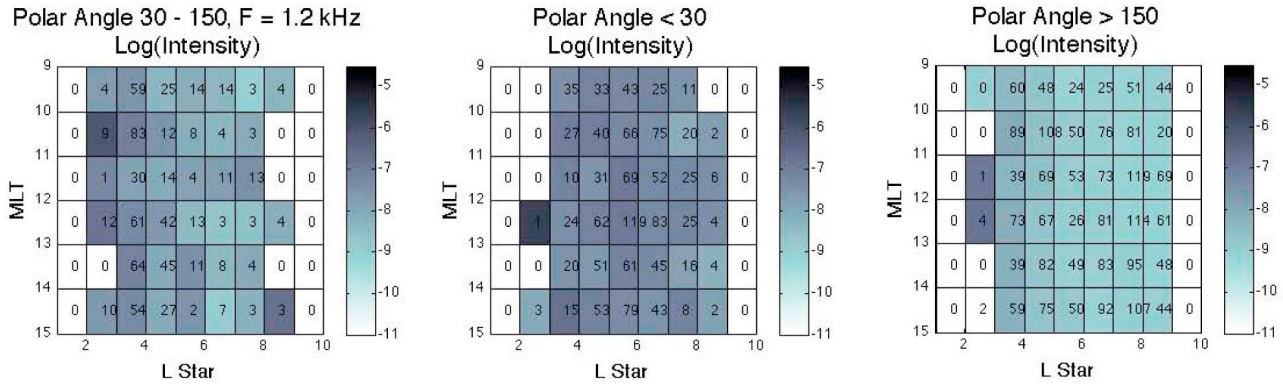

Figure A1. The ~1.2 kHz wave average log intensities for (left) $30° < \theta_{PB0} < 150°$, (middle) $0° < \theta_{PB0} < 30°$, and (right) $150° < \theta_{PB0} < 180°$.

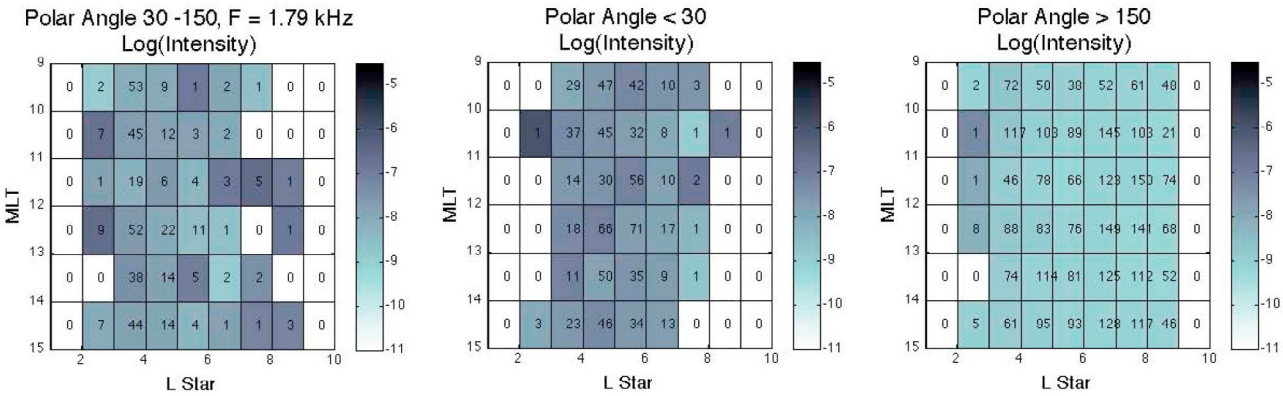

Figure A2. The same format as Figure A1 for ~1.8 kHz waves.

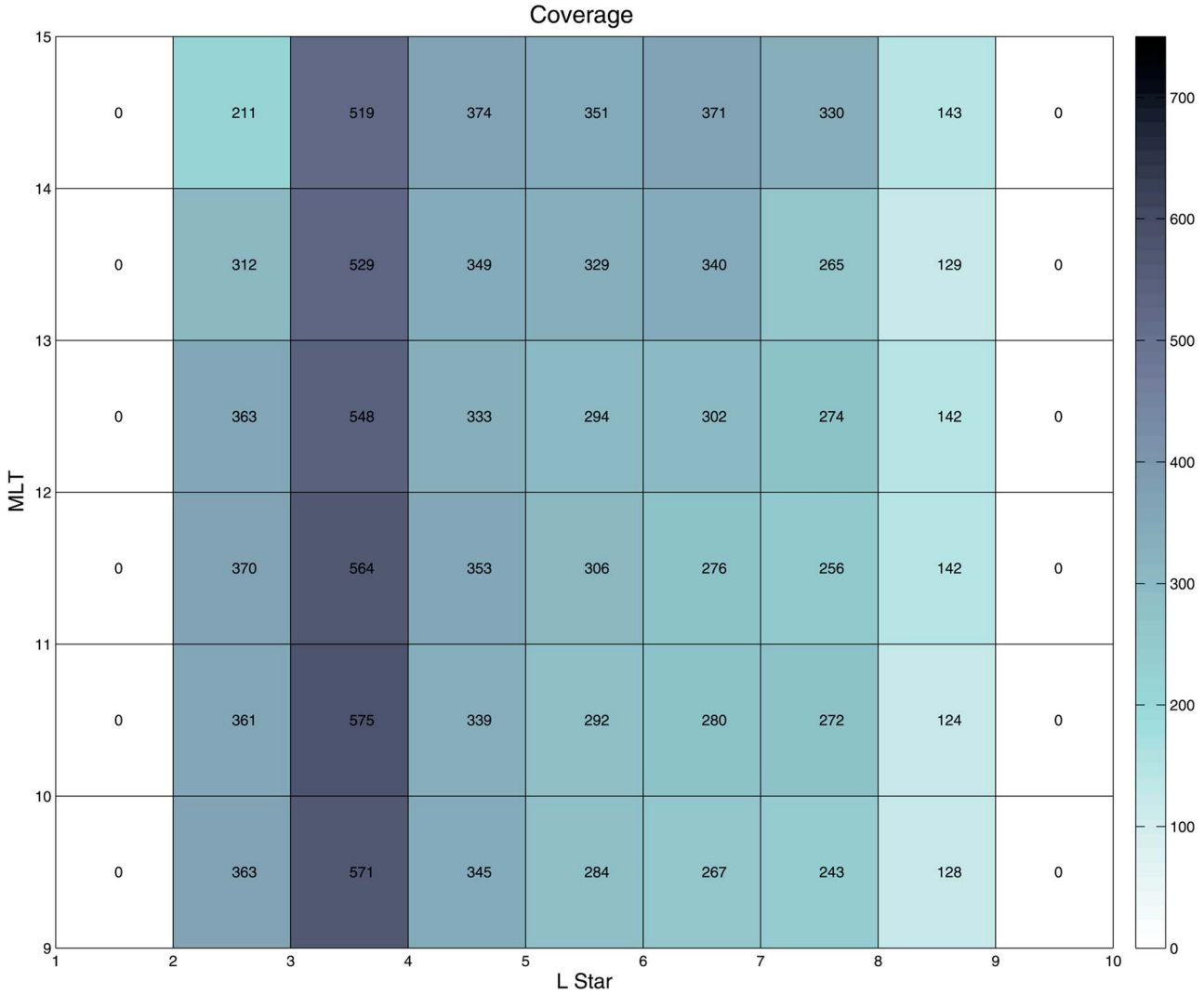

Figure A3. The number of satellite wave interval passes through each ΔL*-ΔMLAT bin. Using the numbers in this figure and those in Figures A1 and A2, the statistics of ∼1.2 kHz and ∼1.8 kHz wave events can be calculated.

format so that the number of wave events can be displayed for each ΔL*-ΔMLAT bin.

[58] Figure A2 has the same format as Figure A1. Figure A2 shows the ∼1.8 kHz wave average log intensities for each ΔL*-ΔMLAT bin.

[59] To give Figures A1 and A2 context, Figure A3 shows the number of satellite wave interval passes through each ΔL*-ΔMLAT bin. Using the numbers in this figure and those in Figures A1 and A2, the statistics of ∼1.2 kHz and ∼1.8 kHz wave events can be calculated.

[60] These figures and Appendix A have been added upon request of one of the referees. This was excluded from the body of the text to conserve space.

[61] **Acknowledgments.** Portions of this work were performed at the Jet Propulsion Laboratory, California Institute of Technology under contract with NASA. GSL thanks the Indian National Science Academy, New Delhi, for support under the Senior Scientist Scheme. JSP and OS acknowledge JPL support under Subcontract 1246597. OS acknowledges additional support from grants GACR 105/10/2279 and ME10001. We acknowledge critical comments given by E. Echer, who helped us discuss interplanetary drivers, and D. Galvan and J. Goldstein for plasmaspheric dynamics, respectively. We thank the two referees for their critical and constructive comments which have helped improve this work.

[62] Robert Lysak thanks the reviewers for their assistance in evaluating this paper.

References

Albert, J. M. (2000), Gyroresonant interactions of radiation belt particles with a monochromatic electromagnetic wave, *J. Geophys. Res.*, *105*(A9), 21,191.

Albert, J. M. (2002), Nonlinear interaction of outer zone electrons with VLF waves, *Geophys. Res. Lett.*, *29*(8), 1275, doi:10.1029/2001GL013941.

Anderson, R. R., and K. Maeda (1977), VLF emissions associated with enhanced magnetospheric electrons, *J. Geophys. Res.*, *82*, 135, doi:10.1029/JA082i001p00135.

André, R., F. Lefeuvre, F. Simonet, and U. S. Inan (2002), A first approach to model the low-frequency wave activity in the plasmasphere, *Ann. Geophys.*, *20*, 981, doi:10.5194/angeo-20-981-2002.

Bell, T. F., J. P. Luette, and U. S. Inan (1982), ISEE 1 observations of VLF line radiation in the Earth's magnetosphere, *J. Geophys. Res.*, *87*(A5), 3530, doi:10.1029/JA087iA05p03530.

Boardsen, S. A., D. L. Gallagher, D. A. Gurnett, W. K. Peterson, and J. L. Green (1992), Funnel-shaped, low-frequency equatorial waves, *J. Geophys. Res.*, *97*(A10), 14,967.

Bortnik, J., R. M. Thorne, and N. P. Meredith (2008), The unexpected origin of plasmaspheric hiss from discrete chorus emissions, *Nature*, *452*, 62, doi:10.1038/nature06741.

Bortnik, J., W. Li, R. M. Thorne, V. Angelopoulos, C. Cully, J. Bonnell, O. LeContel, and A. Roux (2009a), An observation linking the origin of plasmaspheric hiss to discrete chorus emissions, *Science*, *324*, 775, doi:10.1126/science.1171273.

Bortnik, J., R. M. Thorne, and N. P. Meredith (2009b), Plasmaspheric hiss overview and relation to chorus, *J. Atmos. Sol. Terr. Phys.*, *71*, 1636, doi:10.1016/j.jastp.2009.03.023.

Bortnik, J., L. Chen, W. Li, R. M. Thorne, N. P. Meredith, and R. B. Horne (2011), Modeling the wave power distribution and characteristics of plasmaspheric hiss, *J. Geophys. Res.*, *116*, A12209, doi:10.1029/2011JA016862.

Burtis, W. J., and R. A. Helliwell (1969), Banded chorus—A new type of VLF radiation observed in the magnetosphere by OGO 1 and OGO 3, *J. Geophys. Res.*, *74*, 3002, doi:10.1029/JA074i011p03002.

Burtis, W. J., and R. A. Helliwell (1976), Magnetospheric chorus: Occurrence patterns and normalized frequency, *Planet. Space Sci.*, *24*, 1007, doi:10.1016/0032-0633(76)90119-7.

Carpenter, D. L. (1963), Whistler evidence of a "knee" in the magnetospheric ionization density profile, *J. Geophys. Res.*, *68*, 1675, doi:10.1029/JZ068i006p01675.

Carpenter, D. L. (1966), Whistler studies of the plasmapause in the magnetosphere, *J. Geophys. Res.*, *71*, 693, doi:10.1029/JZ071i003p00693.

Carpenter, D. L., and R. R. Anderson (1992), An ISEE/Whistler model of equatorial electron density in the magnetosphere, *J. Geophys. Res.*, *97*, 1097, doi:10.1029/91JA01548.

Carpenter, D. L., and J. Lemaire (1997), Erosion and recovery of the plasmasphere in the plasmapause region, *Space Sci. Rev.*, *80*, 153.

Chappell, C. R. (1974), Detached plasma regions in the magnetosphere, *J. Geophys. Res.*, *79*, 1861, doi:10.1029/JA079i013p01861.

Chappell, C. R., K. K. Harris, and G. W. Sharp (1970), A study of the influence of magnetic activity on the location of the plasmapause as measured by OGO5, *J. Geophys. Res.*, *75*, 50, doi:10.1029/JA075i001p00050.

Chappell, C. R., K. K. Harris, and G. W. Sharp (1971), The dayside of the plasmasphere, *J. Geophys. Res.*, *76*, 7632, doi:10.1029/JA076i031p07632.

Chen, L., J. Bortnik, R. M. Thorne, R. B. Horne, and V. K. Jordanova (2009), Three-dimensional ray tracing of VLF waves in a magnetospheric environment containing a plasmaspheric plume, *Geophys. Res. Lett.*, *36*, L22101, doi:10.1029/2009GL040451.

Chen, L., J. Bortnik, W. Li, R. M. Thorne, and R. B. Horne (2012), Modeling the properties of plasmaspheric hiss: 2. Dependence on the plasma density distribution, *J. Geophys. Res.*, *117*, A05202, doi:10.1029/2011JA017202.

Chum, J., and O. Santolík (2005), Propagation of whistler-mode chorus to low altitudes: Divergent ray trajectories and ground accessibility, *Ann. Geophys.*, *23*, 3727, doi:10.5194/angeo-23-3727-2005.

Chum, J., F. Jiricek, and J. Smilauer (2005), Nonducted propagation of chorus emissions and their observations, *Planet. Space Sci.*, *53*, 307, doi:10.1016/j.pss.2004.09.057.

Church, S. R., and R. M. Thorne (1983), On the origin of plasmaspheric hiss: Ray path integrated amplification, *J. Geophys. Res.*, *88*, 7941, doi:10.1029/JA088iA10p07941.

Clilverd, M. A., N. P. Meredith, R. B. Horne, S. A. Glauert, R. R. Anderson, N. R. Thomson, F. W. Menk, and B. R. Sandel (2007), Longitudinal and seasonal variations in plasmaspheric electron density: Implications for electron precipitation, *J. Geophys. Res.*, *112*, A11210, doi:10.1029/2007JA012416.

Edgar, B. C. (1976), The upper- and lower-frequency cutoffs of magnetospherically reflected whistlers, *J. Geophys. Res.*, *81*, 205.

Furuya, N., Y. Omura, and D. Summers (2008), Relativistic turning acceleration of radiation belt electrons by whistler mode chorus, *J. Geophys. Res.*, *113*, A04224, doi:10.1029/2007JA012478.

Grebowsky, J. M. (1970), Model study of plasmapause motion, *J. Geophys. Res.*, *75*, 4329, doi:10.1029/JA075i022p04329.

Gurnett, D. A. (1976), Plasma wave interactions with energetic ions near the magnetic equator, *J. Geophys. Res.*, *81*, 2765, doi:10.1029/JA081i016p02765.

Gurnett, D. A., et al. (1995), The Polar plasma wave instrument, *Space Sci. Rev.*, *71*, 597, doi:10.1007/BF00751343.

Haque, N., M. Spasojevic, O. Santolík, and U. S. Inan (2010), Wave normal angles of magnetospheric chorus emissions observed on the Polar spacecraft, *J. Geophys. Res.*, *115*, A00F07, doi:10.1029/2009JA014717.

Hayakawa, M., and S. S. Sazhin (1992), Mid-latitude and plasmaspheric HISS: A review, *Planet. Space Sci.*, *40*, 1325, doi:10.1016/0032-0633(92)90089-7.

Horne, R. B. (2002), The contribution of wave-particle interactions to electron loss and acceleration in the Earth's radiation belts during geomagnetic storms, in *Review of Radio Science 1999–2002*, edited by W. R. Stone, p. 801, IEEE Press, Piscataway, N. J.

Horne, R. B. (2007), Acceleration of killer electrons, *Nat. Phys.*, *3*, 590, doi:10.1038/nphys703.

Horne, R. B., G. V. Wheeler, and H. S. C. K. Alleyne (2000), Proton and electron heating by radially propagating fast magnetosonic waves, *J. Geophys. Res.*, *105*, 27,597, doi:10.1029/2000JA000018.

Horne, R. B., R. M. Thorne, N. P. Meredith, and R. R. Anderson (2003), Diffuse auroral electron scattering by electron cyclotron harmonic and whistler mode waves during an isolated substorm, *J. Geophys. Res.*, *108*(A7), 1290, doi:10.1029/2002JA009736.

Horne, R. B., et al. (2005), Wave acceleration of electrons in the Van Allen radiation belts, *Nature*, *437*, 227, doi:10.1038/nature03939.

Horne, R. B., R. M. Thorne, S. A. Glauert, N. P. Meredith, D. Pokhotelov, and O. Santolík (2007), Electron acceleration in the Van Allen radiation belts by fast magnetosonic waves, *Geophys. Res. Lett.*, *34*, L17107, doi:10.1029/2007GL030267.

Kasahara, Y., H. Kenmochi, and I. Kimura (1994), Propagation characteristics of the ELF emissions observed by the satellite Akebono in the magnetic equatorial region, *Radio Sci.*, *29*, 751, doi:10.1029/94RS00445.

Kasahara, Y., Y. Miyoshi, Y. Omura, O. P. Verkhoglyadova, I. Nagano, I. Kimura, and B. T. Tsurutani (2009), Simultaneous satellite observations of VLF chorus, hot and relativistic electrons in a magnetic storm "recovery" phase, *Geophys. Res. Lett.*, *36*, L01106, doi:10.1029/2008GL036454.

Kennel, C. F., and H. E. Petschek (1966), Limit on stably trapped particle fluxes, *J. Geophys. Res.*, *71*, 1, doi:10.1029/JZ071i001p00001.

Kimura, I. (1966), Effects of ions on whistler-mode ray-tracing, *Radio Sci.*, *1*, 269.

Koons, H. C., and J. L. Roeder (1990), A survey of equatorial magnetospheric wave activity between 5 and 8 R_E, *Planet. Space Sci.*, *38*, 1335, doi:10.1016/0032-0633(90)90136-E.

Koons, H. C., M. H. Dazey, and B. C. Edgar (1978), Satellite observation of discrete VLF line radiation within transmitter-induced amplification bands, *J. Geophys. Res.*, *83*(A8), 3887, doi:10.1029/JA083iA08p03887.

Laakso, H., H. Junginger, A. Roux, R. Schmidt, and C. de Villedary (1990), Magnetosonic waves above f_c (H+) at geostationary orbit: GEOS 2 results, *J. Geophys. Res.*, *95*, 10,609, doi:10.1029/JA095iA07p10609.

Lakhina, G. S., B. T. Tsurutani, O. P. Verkhoglyadova, and J. S. Pickett (2010), Pitch angle transport of electrons due to cyclotron interactions with the coherent chorus subelements, *J. Geophys. Res.*, *115*, A00F15, doi:10.1029/2009JA014885.

Lam, M. M., R. B. Horne, N. P. Meredith, and S. A. Glauert (2007), Modeling the effects of radial diffusion and plasmaspheric hiss on outer radiation belt electrons, *Geophys. Res. Lett.*, *34*, L20112, doi:10.1029/2007GL031598.

Lauben, D. S., U. S. Inan, T. F. Bell, and D. A. Gurnett (2002), Source characteristics of ELF/VLF chorus, *J. Geophys. Res.*, *107*(A12), 1429, doi:10.1029/2000JA003019.

LeDocq, M. J., D. A. Gurnett, and G. B. Hospodarsky (1998), Chorus source locations from VLF Poynting flux measurements with the Polar spacecraft, *Geophys. Res. Lett.*, *25*, 4063, doi:10.1029/1998GL900071.

Li, W., R. M. Thorne, V. Angelopoulos, J. Bortnik, C. M. Cully, B. Ni, O. LeContel, A. Roux, U. Auster, and W. Magnes (2009), Global distribution of whistler-mode chorus waves observed on the THEMIS spacecraft, *Geophys. Res. Lett.*, *36*, L09104, doi:10.1029/2009GL037595.

Meredith, N. P., R. B. Horne, and R. R. Anderson (2001), Substorm dependence of chorus amplitudes: Implications for the acceleration of electrons to relativistic energies, *J. Geophys. Res.*, *106*(A7), 13,165, doi:10.1029/2000JA900156.

Meredith, N. P., M. Cain, R. B. Horne, R. M. Thorne, D. Summers, and R. R. Anderson (2003), Evidence for chorus-driven electron acceleration to relativistic energies from a survey of geomagnetically disturbed periods, *J. Geophys. Res.*, *108*(A6), 1248, doi:10.1029/2002JA009764.

Meredith, N. P., R. B. Horne, M. A. Clilverd, D. Horsfall, R. M. Thorne, and R. R. Anderson (2006), Origins of plasmaspheric hiss, *J. Geophys. Res.*, *111*, A09217, doi:10.1029/2006JA011707.

Meredith, N. P., R. B. Horne, S. A. Glauert, and R. R. Anderson (2007), Slot region electron loss timescales due to plasmaspheric hiss and lightning-generated whistlers, *J. Geophys. Res.*, *112*, A08214, doi:10.1029/2007JA012413.

Meredith, N. P., R. B. Horne, and R. R. Anderson (2008), Survey of magnetosonic waves and proton ring distributions in the Earth's inner magnetosphere, *J. Geophys. Res.*, *113*, A06213, doi:10.1029/2007JA012975.

Meredith, N. P., R. B. Horne, M. M. Lam, M. H. Denton, J. E. Borovsky, and J. C. Green (2011), Energetic electron precipitation during high-speed solar wind stream driven storms, *J. Geophys. Res.*, *116*, A05223, doi:10.1029/2010JA016293.

Moldwin, M. B., L. Downward, H. K. Rassoul, R. Amin, and R. R. Anderson (2002), A new model of the location of the plasmapause: CRRES results, *J. Geophys. Res.*, *107*(A11), 1339, doi:10.1029/2001JA009211.

Němec, F., O. Santolík, K. Gereova, E. Macusova, Y. de Conchy, and N. Cornilleau-Wehrlin (2005), Initial results of a survey of equatorial noise emissions observed by the Cluster spacecraft, *Planet. Space Sci.*, *53*, 291, doi:10.1016/j.pss.2004.09.055.

Němec, F., O. Santolík, K. Gereova, E. Macusova, H. Laakso, Y. de Conchy, M. Maksimovic, and N. Cornilleau-Wehrlin (2006a), Equatorial noise: Statistical study of its localization and the derived number density, *Adv. Space Res.*, *37*, 610, doi:10.1016/j.asr.2005.03.025.

Němec, F., O. Santolík, M. Parrot, and J. J. Berthelier (2006b), Power line harmonic radiation (PLHR) observed by the DEMETER spacecraft, *J. Geophys. Res.*, *111*, A04308, doi:10.1029/2005JA011480.

O'Brien, T. P., and M. B. Moldwin (2003), Empirical plasmapause models from magnetic indices, *Geophys. Res. Lett.*, *30*(4), 1152, doi:10.1029/2002GL016007.

Olsen, R. C., S. D. Shawhan, D. L. Gallagher, J. L. Green, C. R. Chappell, and R. R. Anderson (1987), Plasma observations at the Earth's magnetic equator, *J. Geophys. Res.*, *92*(A3), 2385.

Parrot, M. (1990), World map of ELF/VLF emissions as observed by a low-orbiting satellite, *Ann. Geophys.*, *8*, 135.

Parrot, M., and F. Lefeuvre (1986), Statistical study of the propagation characteristics of ELF hiss observed on GEOS-1, inside and outside the plasmasphere, *Ann. Geophys.*, *4*, 363.

Perraut, S., A. Roux, P. Robert, R. Gendrin, J.-A. Sauvaud, J.-M. Bosqued, G. Kremser, and A. Korth (1982), A systematic study of ULF waves above F_{H+} from GEOS 1 and 2 measurements and their relationships with proton ring distributions, *J. Geophys. Res.*, *87*, 6219, doi:10.1029/JA087iA08p06219.

Pokhotelov, D., F. Lefeuvre, R. B. Horne, and N. Cornilleau-Wehrlin (2008), Survey of ELF-VLF plasma waves in outer radiation belt observed by Cluster STAFF-SA experiment, *Ann. Geophys.*, *26*, 3269.

Ridley, A. J., and M. W. Liemohn (2002), A model-derived stormtime asymmetric ring current driven electric field description, *J. Geophys. Res.*, *107*(A8), 1151, doi:10.1029/2001JA000051.

Rodger, C. J., M. A. Clilverd, N. R. Thomson, R. J. Gamble, A. Seppala, E. Turunen, N. P. Meredith, M. Parrot, J.-A. Sauvaud, and J.-J. Berthelier (2007), Radiation belt electron precipitation into the atmosphere: Recovery from a geomagnetic storm, *J. Geophys. Res.*, *112*, A11307, doi:10.1029/2007JA012383.

Roederer, J. G. (1970), *Dynamics of Geomagnetically Trapped Radiation*, *Phys. and Chem. in Space*, vol. 2, Springer, Berlin, doi:10.1007/978-3-642-49300-3.

Santolík, O., J. S. Pickett, D. A. Gurnett, M. Maksimovic, and N. Cornilleau-Wehrlin (2002), Spatiotemporal variability and propagation of equatorial noise observed by Cluster, *J. Geophys. Res.*, *107*(A12), 1495, doi:10.1029/2001JA009159.

Santolík, O., F. Němec, K. Gereova, E. Macusova, Y. de Conchy, and N. Cornilleau-Wehrlin (2004a), System analysis of equatorial noise below the lower hybrid frequency, *Ann. Geophys.*, *22*, 2587, doi:10.5194/angeo-22-2587-2004.

Santolík, O., D. A. Gurnett, J. S. Pickett, M. Parrot, and N. Cornilleau-Wehrlin (2004b), A microscopic and nanoscopic view of storm-time chorus on 31 March 2001, *Geophys. Res. Lett.*, *31*, L02801, doi:10.1029/2003GL018757.

Santolík, O., J. Chum, M. Parrot, D. A. Gurnett, J. S. Pickett, and N. Cornilleau-Wehrlin (2006), Propagation of whistler mode chorus to low altitudes: Spacecraft observations of structured ELF hiss, *J. Geophys. Res.*, *111*, A10208, doi:10.1029/2005JA011462.

Santolík, O., J. S. Pickett, D. A. Gurnett, J. D. Menietti, B. T. Tsurutani, and O. Verkhoglyadova (2010a), Survey of Poynting flux of whistler mode chorus in the outer zone, *J. Geophys. Res.*, *115*, A00F13, doi:10.1029/2009JA014925.

Santolík, O., D. A. Gurnett, J. S. Pickett, S. Grimald, P. M. E. Decreau, M. Parrot, N. Cornilleau-Wehrlin, F. El-Lemdani Mazouz, D. Schriver, and A. Fazakerley (2010b), Wave-particle interactions in the equatorial source region of whistler-mode emissions, *J. Geophys. Res.*, *115*, A00F16, doi:10.1029/2009JA015218.

Schriver, D., et al. (2010), Generation of whistler mode emissions in the inner magnetosphere: An event study, *J. Geophys. Res.*, *115*, A00F17, doi:10.1029/2009JA014932.

Sheeley, B. W., M. B. Moldwin, and H. K. Rassoul (2001), An empirical plasmasphere and trough density model: CRRES observations, *J. Geophys. Res.*, *106*(A11), 25,631–25,641, doi:10.1029/2000JA000286.

Shprits, Y. Y. (2009), Potential waves for pitch-angle scattering of near-equatorially mirroring energetic electrons due to the violation of the second adiabatic invariant, *Geophys. Res. Lett.*, *36*, L12106, doi:10.1029/2009GL038322.

Sigsbee, K., J. D. Menietti, O. Santolík, and J. S. Pickett (2010), Locations of chorus emissions observed by the Polar Plasma Wave Instrument, *J. Geophys. Res.*, *115*, A00F12, doi:10.1029/2009JA014579.

Smith, E. J., and B. T. Tsurutani (1976), Magnetosheath lion roars, *J. Geophys. Res.*, *81*, 2261, doi:10.1029/JA081i013p02261.

Smith, E. J., A. M. A. Frandsen, B. T. Tsurutani, R. M. Thorne, and K. W. Chan (1974), Plasmasheric hiss intensity variations during magnetic storms, *J. Geophys. Res.*, *79*, 2507, doi:10.1029/JA079i016p02507.

Smith, E. J., B. T. Tsurutani, and R. L. Rosenberg (1978), Observations of the interplanetary sector structure up to heliographic latitudes of 16°: Pioneer 10 and 11, *J. Geophys. Res.*, *83*, 717, doi:10.1029/JA083iA02p00717.

Sonnerup, B. U., and L. J. Cahill Jr. (1967), Magnetopause structure and attitude from Explorer 12 observations, *J. Geophys. Res.*, *72*, 171, doi:10.1029/JZ072i001p00171.

Storey, L. R. O., F. Lefeuvre, M. Parrot, L. Cairo, and R. R. Anderson (1991), Initial survey of the wave distribution functions for plasmaspheric hiss observed by ISEE-1, *J. Geophys. Res.*, *96*(A11), 19,469.

Summers, D., R. M. Thorne, and F. Xiao (1998), Relativistic theory of wave-particle resonant diffusion with application to electron acceleration in the magnetosphere, *J. Geophys. Res.*, *103*, 20,487, doi:10.1029/98JA01740.

Summers, D., C. Ma, N. P. Meredith, R. B. Horne, R. M. Thorne, and R. R. Anderson (2004), Modeling outer zone relativistic electron response to whistler mode chorus activity during substorms, *J. Atmos. Sol. Terr. Phys.*, *66*, 133, doi:10.1016/j.jastp.2003.09.013.

Summers, D., B. Ni, and N. P. Meredith (2007a), Timescales for radiation belt electron acceleration and loss due to resonant wave particle interactions: 1. Theory, *J. Geophys. Res.*, *112*, A04206, doi:10.1029/2006JA011801.

Summers, D., B. Ni, and N. P. Meredith (2007b), Timescales for radiation belt electron acceleration and loss due to resonant wave-particle interactions: 2. Evaluation for VLF chorus, ELF hiss, and electromagnetic ion cyclotron waves, *J. Geophys. Res.*, *112*, A04207, doi:10.1029/2006JA011993.

Thorne, R. M., and C. F. Kennel (1967), Quasi-trapped VLF propagation in the outer magnetosphere, *J. Geophys. Res.*, *72*, 857, doi:10.1029/JZ072i003p00857.

Thorne, R. M., E. J. Smith, R. K. Burton, and R. E. Holzer (1973), Plasmaspheric hiss, *J. Geophys. Res.*, *78*, 1581, doi:10.1029/JA078i010p01581.

Thorne, R. M., S. R. Church, W. J. Malloy, and B. T. Tsurutani (1977), The local time variation of ELF emissions during periods of substorm activity, *J. Geophys. Res.*, *82*, 1587.

Thorne, R. M., S. R. Church, and D. J. Gorney (1979), On the origin of plasmaspheric hiss: The importance of wave propagation during periods of substorm activity, *J. Geophys. Res.*, *84*, 5241, doi:10.1029/JA084iA09p05241.

Tsurutani, B. T., and G. S. Lakhina (1997), Some basic concepts of wave-particle interactions in collisionless plasmas, *Rev. Geophys.*, *35*(4), 491.

Tsurutani, B. T., and E. J. Smith (1974), Postmidnight chorus: A substorm phenomenon, *J. Geophys. Res.*, *79*, 118, doi:10.1029/JA079i001p00118.

Tsurutani, B. T., and E. J. Smith (1977), Two types of magnetospheric ELF chorus and their substorm dependences, *J. Geophys. Res.*, *82*, 5112, doi:10.1029/JA082i032p05112.

Tsurutani, B. T., E. J. Smith, and R. M. Thorne (1975), Electromagnetic hiss and relativistic electron losses in the inner zone, *J. Geophys. Res.*, *80*, 600, doi:10.1029/JA080i004p00600.

Tsurutani, B. T., E. J. Smith, H. I. West Jr., and R. M. Buck (1979), Chorus, energetic electrons and magnetospheric substorms, in *Wave Instabilities in Space Plasmas*, edited by P. J. Palmaesso and K. Papadopoulos, p. 55, D. Reidel, Dordrecht, Netherlands.

Tsurutani, B. T., R. M. Thorne, E. J. Smith, J. T. Golsing, and H. Matsumoto (1987), Steepened magnetosonic waves at comet Giacobini-Zinner, *J. Geophys. Res.*, *92*, 11,074, doi:10.1029/JA092iA10p11074.

Tsurutani, B. T., D. J. Southwood, E. J. Smith, and A. Balogh (1993), A survey of low frequency (LF) waves at Jupiter: The Ulysses encounter, *J. Geophys. Res.*, *98*, 21,203, doi:10.1029/93JA02586.

Tsurutani, B. T., et al. (2006a), Corotating solar wind streams and recurrent geomagnetic activity: A review, *J. Geophys. Res.*, *111*, A07S01, doi:10.1029/2005JA011273.

Tsurutani, B. T., R. L. McPherron, W. D. Gonzalez, G. Lu, J. H. A. Sobral, N. Gopalswamy, and F. L. Guarnieri (2006b), Magnetic storms caused by corotating solar wind streams, in *Recurrent Magnetic Storms: Corotating Solar Wind Streams*, *Geophys. Monogr. Ser.*, vol. 167, edited by B. T. Tsurutani et al., p. 1, AGU, Washington, D. C.

Tsurutani, B. T., O. P. Verkhoglyadova, G. S. Lakhina, and S. Yagitani (2009), Properties of dayside outer zone chorus during HILDCAA events: Loss of energetic electrons, *J. Geophys. Res.*, *114*, A03207, doi:10.1029/2008JA013353.

Tsurutani, B. T., B. J. Falkowski, O. P. Verkhoglyadova, J. S. Pickett, O. Santolík, and G. S. Lakhina (2011), Quasi-coherent chorus properties: 1. Implications for wave-particle interactions, *J. Geophys. Res.*, *116*, A09210, doi:10.1029/2010JA016237.

Verkhoglyadova, O. P., B. T. Tsurutani, Y. Omura, and S. Yagitani (2009), Properties of dayside nonlinear rising tone chorus emissions at large L observed by GEOTAIL, *Earth Planets Space*, *61*, 625.

Verkhoglyadova, O. P., B. T. Tsurutani, and G. S. Lakhina (2010), Properties of obliquely propagating chorus, *J. Geophys. Res.*, *115*, A00F19, doi:10.1029/2009JA014809.

Wang, C., Q. Zong, F. Xiao, Z. Su, Y. Wang, and C. Yue (2011), The relations between magnetospheric chorus and hiss inside and outside the plasmasphere boundary layer: Cluster observations, *J. Geophys. Res.*, *116*, A07221, doi:10.1029/2010JA016240.

Winterhalter, D. N., E. J. Smith, M. E. Burton, N. Murphy, and D. J. McComas (1994), The heliospheric plasma sheet, *J. Geophys. Res.*, *99*, 6667, doi:10.1029/93JA03481.